astro-ph/16 Feb. 2004

DUST IN THE PHOTOSPHERIC ENVIRONMENT II. EFFECT ON THE NEAR INFRARED SPECTRA OF L AND T DWARFS [1]

TAKASHI TSUJI

Institute of Astronomy, School of Science, The University of Tokyo
2-21-1, Osawa, Mitaka, Tokyo, 181-0015, Japan

ttsuji@ioa.s.u-tokyo.ac.jp

TADASHI NAKAJIMA

National Astronomical Observatory
2-21-1 Osawa, Mitaka, Tokyo, 181-8588, Japan

tadashi.nakajima@nao.ac.jp

and

KENSHI YANAGISAWA

Okayama Astronomical Observatory, National Astronomical Observatory
Kamogata, Okayama, 719-0231 Japan

yanagi@oao.nao.ac.jp

ABSTRACT

We report an attempt to interpret the spectra of L and T dwarfs with the use of the Unified Cloudy Model (UCM). For this purpose, we extend the grid of the UCMs to the cases of $\log g = 4.5$ and 5.5. The dust column density relative to the gas column density in the observable photosphere is larger at the higher gravities, and molecular line intensity is generally smaller at the higher gravities. The overall spectral energy distributions (SEDs) are $f_J < f_H < f_K$ in middle and late L dwarfs, $f_J < f_H > f_K$ in early T dwarfs (L/T transition objects), and finally $f_J > f_H > f_K$ in middle and late T dwarfs, where f_J, f_H, and f_K are the peak fluxes at J, H, and K bands, respectively, in f_ν unit. This tendency is the

opposite to what is expected for the temperature effect, but can be accounted for as the effect of thin dust clouds formed deep in the photosphere together with the effect of the gaseous opacities including H_2 (CIA), H_2O, CH_4, and K I. Although the UCMs are semi-empirical models based on a simple assumption that thin dust clouds form in the region of $T_{\rm cr} \lesssim T \lesssim T_{\rm cond}$ ($T_{\rm cr} \approx 1800\,{\rm K}$ is an only empirical parameter while $T_{\rm cond} \approx 2000\,{\rm K}$ is fixed by the thermodynamical data), the major observations including the overall SEDs as well as the strengths of the major spectral features are consistently accounted for throughout L and T dwarfs. In view of the formidable complexities of the cloud formation, we hope that our UCM can be of some use as a guide for future modelings of the ultracool dwarfs as well as for interpretation of observed data of L and T dwarfs.

Subject headings: infrared: stars – molecular processes — stars: atmospheres — stars: fundamental parameters – stars: late-type — stars: low-mass, brown dwarfs —

1. INTRODUCTION

So far, few models are available for interpretation and analysis of the spectra of L and T dwarfs consistently. Especially, it is well recognized that dust forms in the photosphere of L dwarfs, but it is by no means clear how to take the effect of dust into account in the predictions of the spectra and the spectral energy distributions (SEDs). Our initial attempt simply assumed that dust forms everywhere so long as the thermodynamical condition of condensation is met (Tsuji, Ohnaka, & Aoki 1996). Although such models could explain the spectra of late M dwarfs and early L dwarfs (e.g. Jones & Tsuji 1997; Tsuji 2000; Schweitzer et al. 2001), at least qualitatively, they failed to explain the spectra of cooler L dwarfs as well as of T dwarfs. In fact, the photospheres will soon be filled with dust if the simple thermochemical equilibrium including condensation is assumed, and the optical thickness of dust is so large that the predicted spectra from such a model will simply be a blackbody radiation of $T = T_{\rm eff}$ for $T_{\rm eff} \lesssim 1500$K or so (Tsuji 2000, 2001). The fully dusty models by other authors (e.g. Allard et al. 2001) may have the same difficulty. On the other hand, cool T dwarfs, whose prototype is Gl 229B, show no evidence of dust in their spectra. A naive interpretation was that the dust may have segregated from the gaseous mixture and

[1]Based on the data collected at the Subaru Telescope, which is operated by the National Astronomical Observatory of Japan

precipitated below the photosphere (Tsuji et al. 1996b; Marley et al. 1996; Allard et al. 1996; Fegley & Lodders 1996). However, a question is why such segregation of the dust took place only in cool T dwarfs.

As a possibility to resolve such difficulties, we proposed a new model which we referred to as the unified cloudy model, UCM (Tsuji 2001) and extended it to a grid ($\log g$ =5.0 and $800 \leq T_{\rm eff} \leq 2600\,{\rm K}$) for applications to L and T dwarfs (Tsuji 2002; hereafter referred to as Paper I). In the UCMs, the segregation of dust from the gaseous mixture takes place in all the ultracool dwarfs including L and T dwarfs and at about the same temperature referred to as the critical temperature $T_{\rm cr}$. Then, roughly speaking, the dust will remain in the observable photosphere for the relatively warm dwarfs with $T_{\rm eff} > T_{\rm cr}$ (note that $T \approx T_{\rm eff}$ at $\tau \approx 1$ and hence the region of $T \gtrsim T_{\rm cr}$, where dust still survives, is found in the optically thin region), and hence such warm dwarfs as L dwarfs will appear to be dusty. In the cooler dwarfs with $T_{\rm eff} < T_{\rm cr}$, on the other hand, the optically thin region (i.e. $\tau < 1$ and hence $T < T_{\rm eff}$) will be cooler than $T_{\rm cr}$ and all the dust grains there will be segregated and precipitated. For this reason, such cool dwarfs as T dwarfs will appear to be dust-free. It is to be noted that this assumption behind the UCM is physically more natural than to assume that dust once formed never segregate throughout the photosphere (namely the fully dusty model of case B) or all the dust grains segregate as soon as they are formed (i.e. fully dust-segregated model of case C).

The UCM, however, is by no means a self-consistent theoretical model, but rather it is a kind of semi-empirical model at present. It should be emphasized, however, that empirical approach often plays an important role in modeling stellar photospheres and atmospheres, even in the more simple cases where dust plays no role. For example, empirical models are still widely used for the solar photosphere, not to speak of the solar atmosphere (i.e. whole the observable layers including the photosphere, chromosphere, CO-mosphere, transition layer, corona etc.) for which no fully theoretical model may yet exist. Once the phase transition occurs in the photosphere, it will introduce complicated phenomena such as those familiar in the meteorology, and it appears to be more difficult to build a fully theoretical model from the beginning. Instead, we hope to understand the basic features of the dust in L and T dwarfs with the simplest possible semi-empirical model which is consistent with the known observations as well as with the basic physics such as thermodynamics. We notice that some attempts have been made in theoretical modelings of the dust formation in L and T dwarfs (e.g. Ackerman & Marley 2001; Helling et al. 2001; Marley et al. 2002; Copper et al. 2003; Woitke & Helling 2003), but it is not yet clear if they provide consistent interpretation of the major observations throughout L and T dwarfs.

So far, we have already shown that the UCMs provide reasonable account for the L/T

transition on the color-magnitude (CM) diagram (Tsuji & Nakajima 2003) as well as major observations such as infrared colors and spectra of ultracool dwarfs throughout L and T dwarfs (Paper I). This fact implies that the UCMs may represent the physical structure of L and T dwarfs to some extent. As a next step in observational tests of the UCMs, we examine if the calibrated spectra observed with the Subaru Telescope, as detailed in a separate paper (Nakajima, Tsuji, & Yanagisawa 2004), can be fitted with the predicted spectra based on the UCMs. For this purpose, we first discuss some details of the UCMs and extend them to cover the possible range of the surface gravities and effective temperatures (Sect. 2). Next, we discuss the dependence of the observable properties on the basic stellar parameters (Sect. 3). Then we focus our attention on interpreting the spectral energy distributions or the spectra of L, L/T transition objects, and T dwarfs based on a single grid of UCMs (Sect. 4). Although we confirm that the observed spectra can reasonably be accounted for by the UCMs, many problems remain unsolved before a more detailed confrontation between models and observations can be possible (Sect. 5).

2. The Unified Cloudy Models

2.1. Dust in the Unified Cloudy Models

The basic features of the UCMs are essentially based on a simple thermodynamical argument. Namely, the dust forms near the dust condensation temperature $T_{\rm cond}$ as soon as the thermodynamical condition for condensation is met, and dust grows to be as large as the critical radius $r_{\rm cr}$ at which the Gibbs free energy of formation attains the maximum. Since the Gibbs free energy should decrease in any chemical reaction, the dust grains smaller than the critical radius $r_{\rm cr}$ cannot grow larger and are in detailed balance with the ambient gaseous molecules by repeating formation and dissociation forever so long as the thermodynamical condition of condensation is fulfilled. On the other hand, the grains larger than the critical radius $r_{\rm cr}$ will grow larger and eventually segregate from the gaseous mixture. This segregation of dust grains will take place at a slightly lower temperature than the condensation temperature $T_{\rm cond}$ and we referred to it as the critical temperature $T_{\rm cr}$. Then, only small dust grains survive in the photosphere in the temperature range of $T_{\rm cr} \lesssim T \lesssim T_{\rm cond}$ and thus a thin dust cloud is formed. Since $T_{\rm cond} \approx 2000\,{\rm K}$ from the thermochemical data, the dust cloud forms deep in the photosphere with T as high as 2000 K independently of $T_{\rm eff}$. As a result, the dust cloud moves from the optically thin region in L dwarfs to the deeper optically thick region in T dwarfs. This migration of the dust cloud gives a direct effect on the the CM diagram (Tsuji & Nakajima 2003) and possibly on the observed spectra as well.

The critical radius $r_{\rm cr}$ is related to the number of monomers n^* at which the Gibbs free

energy of formation $\Delta G(n)$ (eqn.(5) of Paper I) attains the maximum and

$$n^* = \Big(\frac{8\pi a_0^2 \sigma}{3kT \mathrm{In} S}\Big)^3, \tag{1}$$

where a_0 is the radius of the monomer, σ is the surface tension of the condensed grain, and S is the supersaturation ratio [2]. Then,

$$r_{\rm cr} = a_0 \sqrt[3]{n^*}. \tag{2}$$

Some physical data on dust grains are summarized in Table 1, and the critical radii are estimated on the assumption of a modest supersaturation ratio of $S = 1.1$. It is difficult to know the exact value of S, but this cannot be so large under the high density of the photosphere of cool dwarfs. The resulting values of $r_{\rm cr}$ are 0.01 - 0.02 μm and this result is consistent with the fact that the astronomical grains of about these sizes are known. In the following computations, we assume a unique value of the grain radius $r = 0.01\,\mu$m, and size distribution is not considered. However, so long as the grain sizes are small enough (i.e. $r << \lambda$), it is known that(e.g. van de Hulst 1957)

$$Q_{\rm abs} \propto r, \tag{3}$$

and the mass absorption coefficient is almost independent of the grain size (by eqns.(3), (4), (6), (8), and (9)).

The absorption and scattering cross-sections of a dust grain with radius r are:

$$C_{\rm abs} = \pi r^2 Q_{\rm ext}(1-\gamma), \tag{4}$$

and

$$C_{\rm sca} = \pi r^2 Q_{\rm ext}\gamma, \tag{5}$$

where $Q_{\rm ext}$ and γ are the efficiency factor for extinction and albedo, reaspectively. These data used in our UCMs are based on the optical constants found in the literature referred to in Table 1 and the results are shown in Table 2. The mass of a dust particle is

$$w_{\rm dust} = 4\pi r^3 \rho_{\rm dust}/3, \tag{6}$$

where $\rho_{\rm dust}$ is the density (specific gravity) of the dust species. The mass fraction of dust grains in gram of stellar material is

$$f_{\rm dust} = P_{\rm dust} A_{\rm dust}/q(p_{\rm H} A_{\rm H} + p_{\rm He} A_{\rm He} + p_{\rm H_2} A_{\rm H_2}) \tag{7}$$

[2]Note that eqn.(1) was given as eqn.(6) in Paper I, but was misprinted

where $P_{\rm dust}$ is the fictitious pressure of the refractory element (i.e. Fe, Al, and Si for iron, corundum, and enstatite, respectively) that would appear when the dust grains were fully dissolved to the monoatomic gas, $A_{\rm dust}$ is the molecular weight for the chemical formula of the dust species, and q is the number of the refractory elements in the chemical formula (e.g. $q = 2$ for Al_2O_3) ($p's$ and $A's$ are the partial pressures and molecular weights of the species shown by the suffix). The number of the dust grains in gram of stellar material is

$$n_{\rm dust} = f_{\rm dust}/w_{\rm dust}. \tag{8}$$

Then the absorption and scattering coefficients due to the dust species per gram of stellar material are:

$$\kappa_{\rm dust} = C_{\rm abs} n_{\rm dust}, \tag{9}$$

and

$$\sigma_{\rm dust} = C_{\rm sca} n_{\rm dust}, \tag{10}$$

respectively. In the UCMs, these dust absorption and scattering coefficients are added to the continuous absorption and scattering coefficients, respectively, but only for the layers with $T_{\rm cr} \lesssim T \lesssim T_{\rm cond}$[3].

2.2. Revision and Extension of the Unified Cloudy Models

Within the framework of the classical theory of spectral line formation, the spectra depend on chemical composition, effective temperature, surface gravity, and micro-turbulent velocity. As to the chemical composition, we assume the solar system abundances (Anders & Grevesse 1989; note that the iron abundance is based on the meteorite value rather than the photospheric value), but there was a serious problem in the carbon and oxygen abundances in our initial version of the UCMs (Paper I). The situation is much improved with the latest revisions of the C and O abundances (Allene Prieto, Lambert, & Asplund 2001,2002), and we have updated our UCMs with the new C & O abundances ($\log A_{\rm C} = 8.39$ and $\log A_{\rm O} = 8.69$ on the scale of $\log A_{\rm H} = 12.0$).

Previously we assumed $\log\, g = 5.0$ and $v_{\rm micro} = 1\,{\rm km\ s^{-1}}$ throughout, but the effect of the surface gravity should be examined in the analyses of the observed spectra. For this reason, we have extended our grid to include two sequences of UCMs with $\log g = 4.5$ and 5.5. If the radii of ultracool dwarfs are assumed to be the Jupiter's radius, the cases of log

[3]With this simple modification of the extinction coefficients, any available spectral synthesis code can also be applied to the UCMs.

$g = 4.5, 5.0$, and 5.5 correspond to the masses of 13, 40, and 128 $M_{\rm Jupiter}$, respectively, and thus our extended grid may cover the possible range of ultracool dwarfs. The cases of the lower gravities ($\log g$ = 3.0 - 4.0) that may cover the contracting phases were discussed before (Tsuji 2000), but limited to the extreme cases B and C.

In the UCMs, the critical temperature $T_{\rm cr}$ is left as a free parameter, which is to be estimated empirically. Since $T_{\rm cond}(\approx 2000\,{\rm K})$ is fixed by the thermochemical data, the value of $T_{\rm cr}$ is essentially a measure of the thickness of the dust cloud, which should have a direct observable effect. For example, we showed that the red limits of the infrared colors are redder for the lower values of $T_{\rm cr}$ (i.e., for the thicker dust cloud). We analyzed different infrared photometric systems such as the 2MASS (Kirkpatrick et al. 1999, 2000), MKO (Leggett et al. 2002), and CIT (Dahn et al. 2002) systems (see Tsuji 2001, 2002, and Tsuji & Nakajima 2003, respectively), and the results consistently showed $T_{\rm cr} \approx 1800\,{\rm K}$. We confirm that this conclusion will not be affected by the gravity effect (Sect. 3.3). Although the updated grid of the UCMs with $\log g = 5.0$ are with $T_{\rm cr} = T_{\rm surface}, 1700, 1800, 1850, 1900\,{\rm K}$, and $T_{\rm cond}$ (i.e., the case of $T_{\rm cr} = 1850\,{\rm K}$ is added and the 1600 K case of Paper I is removed), we restricted to the case of $T_{\rm cr} = 1800\,{\rm K}$ in the models for $\log g = 4.5$ and 5.5 (and some models of case C for comparison). The $T_{\rm eff}$ values cover the range between 700 and 2600 K throughout.

As an example of the effect of the surface gravities on the UCMs, we compare the UCMs ($T_{\rm cr} = 1800\,{\rm K}$) of $T_{\rm eff} = 1500\,{\rm K}$ for $\log g = 4.5, 5.0$, and 5.5 in Fig.1. The gas pressures are higher for the higher gravities as expected, but the basic features including the convective structure are essentially the same for models with different gravities. The effect of the surface gravities as well as the effective temperatures on the observable properties are discussed in Sects. 3 and 4.

2.3. Molecular Abundances and Dust Column Densities

As an example of L dwarfs, the vertical distributions of some molecules and dust grains are shown for the UCM ($T_{\rm cr} = 1800\,{\rm K}$) of $T_{\rm eff} = 1800\,{\rm K}$ and $\log g = 5.0$ in Fig. 2a, in which the abscissa shows the logarithms of the partial pressure of molecule and the ordinate represents the logarithms of the optical depth defined by the Rosseland mean opacity, $\log \tau_{\rm Ross}$ (which is decreasing upward). The grain abundance is shown by the fictitious pressure of the refractive element (e.g. Fe or Al) forming the dust grains referred to as $P_{\rm dust}$ in Sect.2.1. In this model, corundum (Al_2O_3) condenses at about 1950 K and iron at about 1850K. But corundum as well as iron segregates already at $T_{\rm cr} = 1800\,{\rm K}$ in our UCM, and thus the iron cloud is quite thin. The geometrical thickness of the corundum cloud is greater than that of the iron cloud, but its effect may be less than the iron cloud because of the lower dust column density

(note that Al is less abundant than Fe by about an order). The condensation temperature $T_{\rm cond}$ of enstatite ($MgSiO_3$) is below 1800 K and silicate cloud does not appear in this model. Also, these thin dust clouds can not induce convection such as seen in the cooler model to be discussed in the following, and the convection zone remains deep in the photosphere below the dust clouds. The abundance of the dust grains at the strict thermodynamical equilibrium is shown by the dotted line. Presently we are not considering the fate of these segregated grains, which, however, result in a drastic decrease of FeH, for example. In this model, carbon is still largely in CO although an appreciable amount of CH_4 is already formed and oxygen is mostly in H_2O throughout the photosphere. These molecules, both above and below the dust clouds, contribute to the spectral line formation (see Fig. 4), since the optical thickness of the clouds is not so large in this model.

As an example of T dwarfs, a similar diagram is shown for the UCM ($T_{\rm cr} = 1800$ K) of $T_{\rm eff} = 1000$ K and $\log g = 5.0$ in Fig.2b. In this cooler model, the gas pressure of the dust forming region is quite high and the condensation temperatures ($T_{\rm cond}$) of iron and corundum are as high as 2200 K. In our simplified assumption of the uniform $T_{\rm cr}$ value throughout, the iron and corudum clouds appear to be rather thick. Enstatite finally appears but at about 1820 K and thus silicate cloud is very thin in this model. All these clouds are already immersed in the optically thick region and provide little observable effect. One possible effect of these dust clouds, however, is that a new convective zone is induced because of the steep temperature gradient due to the large dust opacities (Paper I). Without the dust cloud, the convective zone is situated in the deeper layer, and it should be emphasized that the convection is induced by the dust clouds and not the reverse. In this cool and dense model, carbon is mostly in CH_4 rather than in CO. On the other hand, oxygen not only remains mostly in H_2O but also additional H_2O will be formed by the oxygen released from the dissociation of CO. For this reason, H_2O in Fig. 2a is less abundant than CO while it is more abundant than CH_4 in Fig. 2b (Note that the abundance of CO in Fig. 2a and that of CH_4 in Fig. 2b are both equal to the carbon abundance). These molecules can now be observed without obscuration by the clouds.

The logarithmic ratio of the mass column density of iron grains against that of the total gaseous mixture in the observable photosphere is shown in Fig. 3. For comparison, the logarithm of the mass ratio of Fe to H for the composition assumed is -2.75, and thus maximum of about 10% of Fe in the observable photoshere is in the form of iron grains forming the dust cloud in the present UCMs. The iron cloud first appears in the models of $T_{\rm eff} = 2100, 2200$, and 2400 K for $\log g = 4.5$, 5.0, and 5.5, respectively, and it will be immersed below the observable photosphere in the models of $T_{\rm eff} \lesssim 1200$ K for all the $\log g$ values. However, this does not necessarily imply that the effect of dust cloud suddenly disappears at $T_{\rm eff} \approx 1200$ K, because of the large non-greyness of the opacities. We assumed

the limit of the observable photosphere to be at $\tau_{\rm Ross} = 3$ where it is still not so opaque in the J-band region, since $\kappa_{\rm Ross}$ is dominated by the H_2 collision-induced absorption (CIA) which is very effective in the K-band region. Thus, the definition of the dust column density in the observable photosphere cannot be very accurate, but Fig. 3 will give some idea.

3. PREDICTED PROPERTIES OF THE UNIFIED CLOUDY MODELS

3.1. Spectral Line Intensities

As a guide to interpret the spectra, we evaluate the spectral line intensities familiar in the classical stellar spectroscopy (e.g. Unsöld 1955; Cayrel & Jugaku 1963). For this purpose, we apply the method of weighting function and define the spectral line intensity Γ_λ so that the reduced equivalent width W/λ at the weak line limit is given by

$$\log(W/\lambda) = \log gf + \log\Gamma_\lambda(\chi) \tag{11}$$

with

$$\Gamma_\lambda(\chi) = \frac{\pi e^2}{mc^2}\lambda \int_0^\infty P(\tau_\lambda) G_\lambda(\tau_\lambda) \frac{d\tau_\lambda}{\kappa_\lambda} \tag{12}$$

where κ_λ includes all the background continuous opacities due to ions, atoms, molecules, dust, and quasi-continuous sources (e.g. H_2 CIA, K I lines),

$$G_\lambda(\tau_\lambda) = \frac{2}{F_{\rm cont}(\tau = 0)} \int_{\tau_\lambda}^\infty \frac{dS_\lambda(t)}{dt} E_2(t) dt \tag{13}$$

is the weighting function (S_λ is the source function and E_2 is the integrated exponential function), and

$$P(\tau_\lambda) = \frac{p_{\rm mol}}{P({\rm H})} \frac{1}{u(T)} 10^{-\chi\theta} (1 - e^{-hc/\lambda kT}) \frac{1}{\mu_{\rm H} m_{\rm H}} \tag{14}$$

is the number of molecules per gram of stellar material at the fictitious lower level with statistical weight unity and with the lower excitation potential χ (in eV). Also, $p_{\rm mol}$ is the partial pressure of molecule of interest, $P({\rm H})$ is the fictitious pressure of the hydrogen nuclei, $u(T)$ is the partition function, and $\mu_{\rm H}$ is the mean molecular weight with respect to the hydrogen nuclei.

The resulting line intensities for a line with $\chi = 0.0$ eV in the H_2O 1.4 μm bands are shown in Fig. 4a. If the gf-value is known, the reduced equivalent width at the weak line limit can readily be given by eqn.(11) with log $\Gamma_\lambda(\chi)$ value in Fig. 4a. Inspection of Fig. 4a reveals that the H_2O 1.4 μm bands are weaker for the higher gravities at the same $T_{\rm eff}$ and stronger at lower $T_{\rm eff}$ at the given log g value in general. But the H_2O line intensities show a

dip at about $T_{\rm eff} \approx 1600 - 1700\,{\rm K}$, and this is due to the effect of the dust extinction which is the largest at about these $T_{\rm eff}$ values. We also show the line intensities for a line with $\chi = 0.0$ eV in the H_2O bands near $3.0\,\mu$m in Fig. 4a, in which the dip disappeared. This is because the dust opacity is no longer so important at $3.0\,\mu$m as at $1.4\,\mu$m.

The line intensities for a line with $\chi = 0.0$ eV in the CO $2.3\,\mu$m bands strongly depend on the gravities as shown in Fig.4b. This is due to the effect of H_2 CIA which is most effective in the K band region. Since CIA depends on the square of the density, CO bands suffer serious weakening at the higher gravities. Also, the CO $2.3\,\mu$m bands show rapid decline at about $T_{\rm eff} \approx 1500\,{\rm K}$ and this is due to the formation of methane at about this $T_{\rm eff}$ value. Actually, CO bands may be masked by the stronger CH_4 bands at the cooler $T_{\rm eff}$ values, but such an effect is not taken into account in the present line intensities, since the methane bands are not considered as a background opacity in eqn.(12). In contrast, the line intensities for a line ($\chi = 0.0$ eV) of the CH_4 bands show rapid increase at about $T_{\rm eff} \approx 1500\,{\rm K}$. However, they show only minor dependence on the gravities even though they should also suffer the effect of H_2 CIA. This is because the CH_4 abundance is also highly sensitive to the gravities and this fact may roughly cancel the effect of the increased CIA at the higher gravities.

Finally, as an example of refractory molecules, the line intensities for a line with $\chi = 0.0$ eV in the FeH $1.1\,\mu$m bands are shown in Fig. 4c. Although FeH almost disappears above the iron cloud, it is quite abundant to give a large line intensity in L dwarfs because of the presence of FeH below the iron cloud (Fig. 2a). As the iron cloud migrates to the deeper layer with decreasing $T_{\rm eff}$, all the iron-bearing molecules are swept by the iron cloud and little FeH is left in the observable photosphere above the cloud. Nevertheless, the non-zero line intensities of FeH is found in the models of $T_{\rm eff} \lesssim 1500\,{\rm K}$ (Fig. 4c), and this is due to a small amount of FeH above the iron cloud which is in equilibrium with the solid iron (Fig. 2b). This small amount of FeH may not be sufficient to explain the FeH bands detected in T dwarfs (Burgasser et al. 2002b; Nakajima et al. 2004). Moreover, this small amount of FeH was assumed to be in chemical equilibrium with the iron grains which, however, are assumed to be precipitated already below the photosphere in our UCMs. Thus, this small amount of FeH is not in chemical equilibrium with dust and further analysis should be needed to know the effect of the dust grains assumed to have precipitated in our UCMs. Anyhow, some other mechanism(s) must be considered to explain the FeH bands observed in T dwarfs. One possibility may be a convective dredge-up of FeH abundant below the clouds by the second convective zone (Fig. 1). Such a possibility was also considered but dismissed by Burgasser et al. (2002), who suggested an alternative explanation that the FeH residing below the cloud deck can be seen through holes in the clouds.

The line spectra depend not only on the stratification of the molecule of interest but also on the nature of the background opacities including dust, H_2 CIA, resonance wings of K I and Na I etc in addition to the usual continuous opacities. In the photospheres of ultracool dwarfs, all these quantities show drastic changes with $T_{\rm eff}$, log g, wavelength region etc., and their effect upon the spectral lines can best be investigated by the spectral line intensities outlined above. Of course, all these effects are automatically taken into account in the computation of the synthetic spectra (Sect. 3.2), but the dependence of the spectral features on various physical parameters can be more clearly realized in the simple line intensities. Also, the spectral line intensities can directly be used for abundance analysis if sufficiently weak lines can be measured at high resolution, or can be used as the abscissa of the curves-of-growth for the general cases.

3.2. Synthetic Spectra and Spectral Energy Distributions

In the computation of the spectra, we apply the linelist including H_2O, ^{12}CO, ^{13}CO, OH, SiO, CN, and K I while other molecules including CH_4, NH_3, PH_3, H_2S, CO_2, TiO, and VO are treated as pseudo-continua with the use of the band model method. Now, in applying these spectra to an analysis of the actual spectra, we try some improvements over the previous work (Paper I): First, we now use the linelist of H_2O based on the work of Partridge & Schwenke (1997) instead of the HITEMP database (Rothman 1997) used before. The resulting spectra, however, show rather minor change in the spectral region and at the resolution we are interested in. Second, we change the f_e-value of FeH from 0.013 (Langhoff & Bauschlicher 1990) to an empirical value of 0.001 (Schiavon, Barbuy, & Singh 1997), and the resulting spectra turned out to show better agreement with the observed ones. Also, we replaced the band model opacity with the linelist by Phillips et al. (1987) and with the intensity data by Schiavon et al. (1997), which are both made available by Samner Davis.

Third, the most serious problem is that CH_4 is quite dominant especially in T dwarfs as well as in late L dwarfs, but the band model opacity largely overestimates the methane absorption except for the latest T dwarfs. We then tried the linelist of CH_4 included in the GEISA database (Jacquinet-Husson et al. 1999) but it generally underestimates the methane absorption, since it is mainly for application to the Earth's atmosphere of $T \approx 300$ K. We have no final solution for methane opacity at present and we apply the two alternative methods: one using the band model opacity of CH_4 as well as of FeH and the other the linelists for CH_4 as well as FeH, which we refer to as as case I and case II, respectively. The resulting predicted spectra or spectral energy distributions (SEDs) are discussed in Sect. 4 in comparison with the observed spectra.

3.3. Infrared Colors

With the synthetic spectra or SEDs discussed in Sect. 3.2, integrated flux over a filter band can be evaluated by applying an appropriate filter response function. As an example, we apply the filter response function $S_{\rm band}(\lambda)$ of the MKO system (Tokunaga, Simon, & Vacca 2002; Simon & Tokunaga 2002) to $F(\lambda)$ based on the UCMs ($T_{\rm cr} = 1800\,{\rm K}$) and evaluate

$$F_{\rm band} = \int_{\lambda_1}^{\lambda_2} S_{\rm band}(\lambda) F(\lambda) d\lambda, \tag{15}$$

where λ_1 and λ_2 are the lower and upper limits, respectively, of the response function. We apply the case I methane opacity, which better reproduces the CH_4 bands where they give the most serious effect on $F(\lambda)$, i.e. in T-dwarfs (Sect. 4).

The resulting integrated band fluxes F_J, F_H, and F_K (in unit of erg s^{-1} cm^{-2}) are given in Table 3 on logarithmic scale, which can be applied to estimate the infrared colors and infrared bolometric corrections. For example, $J-K$ can be given by

$$(J-K)_{\rm MKO} = -2.5(\log F_J - \log F_K) + C, \tag{16}$$

where the constant is determined to be $C = 1.328$ so that $(J-K)_{\rm MKO} = 0.0$ for Vega by the use of the integrated band fluxes for the model of $T_{\rm eff} = 9550\,{\rm K}$ and $\log g = 3.95$ (Kurucz 1993), also given in Table 3. The resulting values of the $J-K$ index for the three $\log g$ values are shown in Fig.5, which is an updated version of Fig. 8b (Paper I) for the $\log\, g = 5.0$ models. Inspection of Fig. 5 reveals that $J-K$ is redder for the higher gravities in the L dwarf regime and this can be understood by the gravity effect of the dust mass column densities discussed in Sect. 2.3 (Fig.3). Also, the red limit of $J-K$ is almost independent of the gravity and thus our estimation of the value of $T_{\rm cr}$ based on the red limit of $J-K$ can now be deemed as well confirmed for the possible range of gravities of L and T dwarfs.

4. OBSERVED VS. PREDICTED SPECTRA OF L AND T DWARFS

The computation of the spectra is done with the step of $0.1\,{\rm cm}^{-1}$ for the spectral interval between 0.8 and $2.6\,\mu$m, and the resulting spectra are convolved with the slit function which is assumed to be the Gaussian with FWHM $= 500\,{\rm km\ s}^{-1}$. We assumed $T_{\rm cr} = 1800\,{\rm K}$ throughout. We have tried other values of $T_{\rm cr}$ but no improved fit could be obtained in general, and we do not think that it is useful to fine tune such a parameter case by case at present.

4.1. Middle L Dwarfs

We have no sample of the early L dwarfs and we start with the middle L dwarfs of L3 - L6.5. Since methane may not be prominent in these L dwarfs, we are not bothered by the poorly known data on methane. However, we apply the case II opacities (use linelist of CH_4 and FeH), since CH_4 is already abundant in the models with $T_{\rm eff}$ as high as 1800K (Fig.2a) and methane bands will appear if the methane opacity is overestimated by the case I opacities (use the band model opacity for CH_4 and FeH).

As an example, the observed spectrum of the L6.5 dwarf 2MASS 1711+22 shown by the filled circles is compared with the predicted ones based on the UCMs of five different sets of $T_{\rm eff}$ and $\log g$ in Fig. 6. The best fit is obtained for $T_{\rm eff} = 1800\,{\rm K}$ and $\log g = 5.0$ shown by the solid line in Fig. 6c. For comparison, the predicted spectrum based on our model of case C, in which dust clouds are effectively cleared up, is shown for the same $T_{\rm eff}$ and $\log g$ by the dashed line. The difference of the solid line against the dashed line shows the effect of thin dust clouds formed in the layer of $T_{\rm cr} \lesssim T \lesssim T_{\rm cond}$ in the UCM. Clearly the effect of the dust extinction is the largest in the J band region and is still appreciable in the H band region compared with that in the K band region. Thus the effect of the dust clouds is appreciable even though the dust clouds are rather thin at $T_{\rm eff} \approx 1800\,{\rm K}$ (Fig. 2a).

The effects of changing $T_{\rm eff}$ by $\pm 100\,{\rm K}$ at the same $\log g$ are shown in Figs. 6b and d, and the fits are worse at the J band (note that we first matched the observed and predicted spectra at the K band in general). The strengths of molecular bands including the 1.4 and 1.9 μm H_2O bands as well as the CO first overtones at 2.3 μm can be reasonably well reproduced by all the UCMs of $\log g = 5.0$ shown in Fig. 6.

The effect of changing $\log g$ by +0.5 at $T_{\rm eff} = 1900\,{\rm K}$ is shown in Fig. 6a and a reasonable fit of the overall SED is recovered. However, the molecular bands turn out to be weaker than in the case of $\log g = 5.0$ at the same $T_{\rm eff}$ (Fig. 6b). Also, the effect of changing $\log g$ by -0.5 at $T_{\rm eff} = 1700\,{\rm K}$ is shown in Fig. 6e; the fit of SED is again recovered but the molecular bands appear to be strengthened compared with the case of $T_{\rm eff} = 1700\,{\rm K}$ and $\log g = 5.0$ (Fig. 6d). Thus the molecular bands are weaker at the higher gravities, which is consistent with the results outlined in Sect. 3.1 (Fig. 4), and SED shows larger extinction at the higher gravities as can be understood by the gravity effect on the dust column densities noted in Sect. 2.3 (Fig. 3).

Although the overall fit of the observed data of 2MASS 1711, viewed both as SED and as spectrum, can be obtained for the predicted spectrum based on the UCM with $T_{\rm eff} = 1800\,{\rm K}$ and $\log g = 5.0$, a noticeable gap is found at the peak of the H band; the observed spectrum is rather flat with some absorption features while the predicted spectra show a smooth convex

feature. A possible contribution of the FeH $E^4\Pi - A^4\Pi$ system to the absorption features in the H band region is known (Wallace & Hinkle 2001; Cushing et al. 2003; Nakajima et al. 2004), but we could not include this system in our predicted spectra because of the lack of the necessary spectroscopic data. Also, it is not sure if all the absorption features can be explained by FeH and it is quite possible that other unknown sources will be important.

A more or less similar analysis is done for the spectra of 2MASS 1146+22 (L3), 2MASS 1507-16 (L5), SDSS 2249+00 (L5), and 2MASS 0920+35 (L6.5), which were also observed with the Subaru (Nakajima, Tsuji, & Yanagisawa 2001). The results are shown in Fig. 7 in which the meanings of the solid and dotted lines are the same as in Fig. 6c. The observed spectrum of 2MASS 1146 (L3V) can be fitted slightly better with the predicted one for $T_{\rm eff} = 1900\,{\rm K}$ and $\log g = 5.5$ rather than that for $T_{\rm eff} = 1850\,{\rm K}$ and $\log g = 5.0$. This is consistent with a possibility that the early L dwarf such as 2MASS 1146 is a main-sequence star rather than a brown dwarf as is suggested elsewhere (Nakajima et al. 2004). Also, we show the case of $T_{\rm eff} = 1850\,{\rm K}$ and $\log g = 5.0$ for 2MASS 1507 (L5) rather than the case of $T_{\rm eff} = 1900\,{\rm K}$ and $\log g = 5.5$. The short segment of the spectrum of SDSS 2249 (L5) can roughly be fitted with the predicted one based on the UCM with $T_{\rm eff} = 1800\,{\rm K}$ and $\log g = 5.0$, and a slightly lower gravity may improve the fit. An interesting feature is that the H band region can be accounted for rather well by the UCM for this object, while it is more difficult to account for the H band spectra of other objects as noted already.

In conclusion, the basic features of these L dwarfs shown in Fig. 7 are rather similar to those of 2MASS 1711 (L6.5) shown in Fig. 6, and the overall SED as well as the strengths of the most molecular bands can be fitted with the UCMs of $T_{\rm eff} \approx 1800 - 1900\,{\rm K}$. One unsolved problem in these fits is the gap at the H band region except for SDSS 2249.

4.2. Late L Dwarfs

The detailed comparison of the observed spectra of L dwarfs revealed that the H_2O bands at 1.1 and 1.4 μm are not necessarily stronger in the L8 dwarf 2MASS 1523+30 than in the L5 and L6.5 dwarfs, but the CH_4 bands at 2.2 μm can be identified in the L8 dwarf (Nakajima et al. 2004) as well as the stronger bands at 3.3 μm (Noll et al. 2000). We found that the overall SED as well as the molecular bands of 2MASS 1523 (L8) can be fitted reasonably well with the predicted spectrum based on the UCM of $T_{\rm eff} \approx 1500\,{\rm K}$ and $\log g \approx 5.0$ as shown in Fig. 8. The water bands based on the UCMs are rather weak possibly because of the large dust extinction. In fact, the dust column density in the observable photosphere is the largest at about $T_{\rm eff} \approx 1500\,{\rm K}$ (Fig. 3) and this fact results in a very large difference of the emergent spectra based on the UCM (solid lines) and those based on the dust-segregated

models of case C (dashed lines). Because of this large dust extinction, H_2O 1.1 μm bands as well as K I 1.2 μm doublet are rather weak in the L8 dwarf 2MASS 1523.

We have applied two different opacities for the methane bands (Sect. 3.2); the band model opacity (case I) and the line-by-line opacity (case II), which may provide the maximum and minimum estimates of the real opacity, respectively. The predicted spectra show bifurcation in the 1.6 and 2.2 μm regions and the observed spectrum should appear between the high and low estimates of the emergent spectra. This expectation is met in the 2.2 μm bands, but it is clear that the band model opacity (case I) highly overestimated the methane bands. On the other hand, the predicted spectra based on the available linelist of CH_4 (case II) provides a reasonable fit to the observed 2.2 μm CH_4 bands. The predicted H fluxes are slightly higher than the observed and it is possible that the unknown opacity prevailing in the H band region of L3 - L6.5 dwarfs noted in Sect. 4.1 may have some effect at L8 as well. It is to be noted, however, that the 1.63 and 1.67 μm absorption features can be seen both in the observed and predicted (case II) spectra.

4.3. Early T dwarfs or L/T Transition Objects

SDSS 1254-01 is one of the three remarkable objects whose infrared colors and spectra are both intermediate between the late L dwarfs and cool T dwarfs (Leggett et al. 2000), and SDSS 1254 is now classified as T2 (Burgasser et al. 2002a). The predicted spectra based on the UCMs with $T_{\rm eff} = 1400, 1300$, and 1200 K are shown in Fig. 9, and the effect of dust extinction decreases in this order as evidenced by the decreasing difference between the solid and dashed lines whose meanings are as noted already. On the other hand, the predicted intensities of the molecular bands increase according as the $T_{\rm eff}$ decreases. The best fits, both in the overall SED and in the molecular band strengths, are found for the case of the UCM with $T_{\rm eff} \approx 1300$ K and $\log g \approx 5.0$. The observed methane bands, both at 1.6 and 2.2 μm, are just between the predictions based on the cases I and II opacities.

In our UCMs, the dust cloud is partly immersing into the optically thick region in the early T dwarfs, and this is due to a natural consequence that the dust condensation temperature is just near the optical depth unity at about this spectral type. As a result, the effect of dust extinction is not so large as in the late L dwarfs while volatile molecules including CH_4 can be formed in the layer above the dust clouds. Also, the position of SDSS 1254 on the CM diagram could be reasonably well reproduced by our UCMs with the same value of $T_{\rm cr} = 1800$ K (Tsuji & Nakajima 2003). Thus it should be emphasized that the very simple assumption in our UCMs that the segregation of the dust grains takes place at about $T_{\rm cr} \approx 1800$ K throughout L and T dwarfs accounts for the rapid bluing in the L/T

transition as well as the rather unique spectra of the transition object.

4.4. Middle T dwarfs

The observed spectrum of the T3.5 dwarf SDSS 1750+17 is compared with the predicted ones of $T_{\rm eff} = 1200, 1100$ and 1000 K in Fig. 10. The overall SED appears to be fitted reasonably well with the UCM of $T_{\rm eff} \approx 1100$ K and $\log g \approx 5.5$, and the higher gravity is preferred to explain the rather weak water bands. The predicted water bands still appear to be stronger than the observed ones, and it is possible that the chemical composition of this object may be non-solar. The observed methane bands are well between cases I and II, but the 1.6 μm bands are closer to case I while the 2.2 μm bands to case II. At these low effective temperatures, the effect of dust clouds is rather minor as can be seen in that the SEDs for the cases with and without cloud, shown by the solid and dashed lines, respectively, do not differ significantly. Also, the overall SED can be fitted with the cloud-free model of $T_{\rm eff} = 1200$ K (dashed line in Fig. 10a). It is difficult to judge which of these different cases provides the better fit to the observation. However, the presence of the dust cloud is indispensable for L and early T dwarfs, and we think that it is reasonable to assume the same models for the later T dwarfs as well.

The observed spectrum of the T3.5 dwarf SDSS 1750 may look rather similar to that of SDSS 1254 except that the methane bands are stronger. The overall SED of SDSS 1750, however, is definitively different from those of the L and L/T transition objects and already shows the typical characteristic of T dwarfs in that the flux peaks (in f_ν unit) at J, H, and K bands decrease in this order, namely $f_J > f_H > f_K$ (also see Fig. 11). For comparison, L dwarfs show just the opposite in that $f_J < f_H < f_K$ (see Figs. 6 - 8), and the L/T transition object SDSS 1254 shows the intermediate behavior of L and T dwarfs in that the H flux is the highest, namely $f_J < f_H > f_K$ (see Fig. 9). These gross features are well reproduced by our UCMs (solid lines throughout Figs. 6-11 with the case I methane opacity to the 1.6 μm methane bands in T dwarfs). It is to be noted that the SEDs show $f_J > f_H > f_K$ throughout L and T dwarfs if there is no cloud (i.e. our case C shown by the dashed lines throughout Figs. 6 - 11) because of the large infrared opacity due to H_2 CIA in ultracool dwarfs. The depressions of the J flux in the L/T transition objects and further of the H flux in the L dwarfs are due to the rise of the dust clouds to the optically thin region, which is a natural consequence of the basic assumption of UCM that the dust clouds form only in the region of $T_{\rm cr} \lesssim T \lesssim T_{\rm cond}$.

4.5. Late T dwarfs

We include the classical T dwarf Gl 229B (T6), the observed spectrum (Geballe et al. 1996) of which is found to show a reasonable fit to the predicted one based on the UCM with $T_{\rm eff} = 900\,{\rm K}$ and $\log\,g = 5.0$ as shown in Fig.11a. The observed methane bands at $2.2\,\mu$m are still between the predicted ones based on the cases I and II methane opacities, but the $1.6\,\mu$m bands can be fitted with the predicted spectrum based on the band model opacity (i.e. case I). In a recent paper, Burrows et al. (2002) showed that the spectrum of Gl 229B in the short wavelength region near $1\,\mu$m could be fitted with their models of $T_{\rm eff} = 950\,{\rm K}/\log g = 5.5$ as well as of $T_{\rm eff} = 750\,{\rm K}/\log g = 5.0$. We could fit the same region with our model of $T_{\rm eff} = 900\,{\rm K}/\log g = 5.0$, and slightly different results may be partly because we are still using the classical Lorentzian profiles for the K I opacity, while a more sophisticated theory of the line broadening must be called for (Burrows, Marley, & Sharp 2000; Burrows & Volobuyev 2003).

For the latest T dwarf in our sample, 2MASS 1217-03 (T7.5), the methane bands, both at 1.6 and $2.2\,\mu$m, can roughly be accounted for by the band model opacity (case I) rather than the line-by-line opacity (case II) as shown in Fig. 11b. The spectrum of 2MASS 1217 shows stronger bands of methane as well as of water than in Gl 229B, and can be fitted with the predicted spectrum based on the lower $T_{\rm eff}$ of 800 K and the lower gravity of $\log g = 4.5$, as in Fig. 11b. Also, the same spectrum can marginally be fitted with the predicted one based on the higher $T_{\rm eff}$ of 900 K and the higher gravity of $\log\,g = 5.0$. It is interesting that the same observed spectrum can be fitter either by higher $T_{\rm eff}$/ higher gravity or by lower $T_{\rm eff}$/lower gravity (see also Fig.6), and the same effect was shown by Burrows et al. (2002) as noted above for Gl 229B. Thus accurate estimation of gravity from the infrared spectrum may be difficult unless $T_{\rm eff}$ can be determined by other methods.

In the model of $T_{\rm eff} \lesssim 1000\,{\rm K}$, the predicted spectrum based on our UCMs differs little from that of the fully dust-segregated model of case C as noted in Sect. 4.4. Thus, dust clouds give almost no effect on the observed spectrum once the immersion of the dust clouds in the optically thick regime is completed in these very cool models. This result is consistent with the earlier observations by Liebert et al. (2000) who showed that dust gives little effect on the observed spectrum of the late T dwarf SDSS 1624+00. Thus our previous proposition that the warm dust, together with the the K I and Na I resonance lines, may produce observable effect on the spectra of cool T dwarfs such as Gl 229B (Tsuji, Ohnaka, & Aoki 1999) cannot be supported, even if the warm dust clouds exist in the deeper layer. This result implies that observational studies of dust in cool T dwarfs should be quite difficult.

5. DISCUSSION

5.1. Modeling

The UCM used in this paper is a kind of semi-empirical models rather than a fully consistent theoretical model. This approach is based on the recognition that it should be more difficult to treat all the processes taking place in the dusty photosphere in which phase changes in gas, liquid, and solid may induce complicated chaotic phenomena. An extreme case is the Earth's atmosphere which embraces all the complicated phenomena treated by another big field of science - meteorology. Instead of pursuing the detailed microscopic processes of dust formation and destruction, we tried to approximate the resulting possible structure of the cloudy photosphere by a model to be treated within the framework of the classical non-grey theory. For this purpose, we introduced a simple assumption that the dust grains formed at its condensation temperature will soon grow too large to be sustained in the photosphere at a slightly lower temperature which we referred to as the critical temperature. The only parameter introduced in our semi-empirical approach is the critical temperature, in addition to the mixing length which is assumed to be one pressure scale height in treating convection.

We should certainly do our best to minimize the number of free-adjustable parameters in such a semi-empirical approach, since any observed data may be "explained" if many parameters are assumed. In this paper, we tried to see to what extent the UCMs with the empirically fixed unique value of $T_{\rm cr} = 1800\,{\rm K}$ throughout can explain the available observed spectra. It was not expected from the beginning that the fits can be perfect for such a simplified treatment, and further because of the many approximations both in the model itself as well as in the input data (Sect. 5.2). Nevertheless the overall characteristics of the SEDs as well as the major spectroscopic features of L and T dwarfs can be reasonably accounted for (Figs.6-11). Also, infrared colors (Paper I), L/T transition (Tsuji & Nakajima 2003), and L-T spectral classification (Tsuji 2003; Nakajima et al. 2004) can reasonably be interpreted with the UCMs. Thus, the basic assumption of the UCMs can be deemed as well supported by the observations.

What is important to conclude from the reasonable agreement between the major observational data of L-T dwarfs and predictions from the UCMs is that the dust should certainly form in the photospheres of cool dwarfs but only a small amount of dust should be sufficient. In fact, if dust forms in the full amount as predicted by the thermochemistry, the photosphere will soon be filled in by dust in the cooler brown dwarfs and its spectrum will look like a blackbody as in our case B models (e.g. Paper I). Also this small amount of dust should be concentrated rather deep in the photosphere, since its effect should appear in the coolest

T dwarfs if a small amount of dust is distributed uniformly throughout the photosphere. For this reason, we assumed that the dust should be in the form of a thin cloud deep in the photosphere. The idea that a finite-thickness cloud could explain the approximate shape of the M_J vs. $J-K$ diagram was also proposed by Marley (2000) based on a different approach. Thus the next problem in modeling is to understand why the photospheres of cool dwarfs adjust themselves in such a way as to produce only a small amount of dust in a form of the thin cloud.

As a possible mechanism to produce the cloud, convection may play a role as discussed by several authors (e.g. Ackerman & Marley 2001; Helling et al. 2001; Marley et al. 2002; Copper et al. 2003). One interesting feature is that the particle sizes can be determined by considering the time scale of the convective dredge-up of the raw material to the dust forming region. However, the convective zone is situated rather deep in the photosphere (e.g. Burrows et al. 1997; Allard et al. 2001; Tsuji 2002), and it is not necessarily possible that the convection will reach so nicely to the dust forming region in all the models of L and T dwarfs. The present convective models are based on the mixing-length theory (MLT), but recent detailed 2D and 3D hydrodynamical simulations of surface convection in a late M-dwarf (Ludwig, Allard, & Hauschild 2002) confirmed that the classical MLT allows reasonably accurate prediction of the thermal structure of the late M dwarf and that overshooting extends the convective mixing region only modestly (about 2 pressure scale heights) beyond the Schwarzschild boundary. The possible interplay between convection and cloud formation may be an interesting subject to be pursued further, but our assumption in UCMs is that the thermodynamical constraint, as the first approximation, determines the basic feature of the dusty photospheres.

5.2. Input Data

Apart from the fundamental problem in modeling, the input data are still far from satisfactory. One serious problem is the methane opacity. Although it appeared that the presently available linelist roughly accounts for the observed intensities of the 2.2 μm bands throughout late L to middle T dwarfs (Figs. 8-10), this may be only fortuitous. In fact, the details of the predicted spectra based on the present linelist (Jacquinet-Husson et al. 1999) can never be fitted well with the observed spectra, as shown in Fig. 12 for SDSS 1750 as an example. Inspection of Fig. 12 reveals that only a limited number of predicted bands show correspondences with the observed ones, and it is clear that many bands are missing in the present linelist. Our previous conclusion that the band model opacity may be preferred (Paper I) is only applicable to late T dwarfs in which methane bands are quite strong, as

is confirmed in the coolest T dwarf 2MASS 1217 in our sample (Fig. 11b), but cannot be justified for most cases as are evident in Figs. 6 - 10.

While the problem of molecular opacities can be solved mostly if a more complete linelist can be provided either by experiments or by theories, the case of the dust opacities may be more difficult, since it is closely related to the cloud formation itself. For example, the chemical equilibrium abundance pattern of the dust grains in the stratified clouds suffers the effect of depletion (Lodders 1999) and the so-called rainout (Burrows & Sharp 1999). Also, the equilibrium gas and dust chemistry at low temperatures is quite complicated and involves many problems that require detailed analyses (e.g. Lodders & Fegley 2002; Lodders 2002). Also, possible effects such as due to impurities (the so-called dirty grains) and the core-mantle structures may introduce further difficulties. It is not possible to incorporate all these complications in the present modeling and we restricted ourselves to consider only a few most abundant condensates as noted in Paper I. Probably, it should be required to consider the dust opacities more carefully to have a better fit between observed and predicted SEDs. Unfortunately, it is more difficult to improve the situation because dust, unlike atoms and molecules, shows few direct spectroscopic features and thus it is very difficult to have empirical assessments on the dust opacities.

5.3. Applications

The effective temperatures corresponding to the best fits between the observed and predicted spectra discussed in Sect. 4 are summarized in Table 4 as $T_{\rm eff}$(SED). Although the resulting values of $T_{\rm eff}$ show little change within the middle L dwarfs (L3 - L6.5), they show steady decrease to the late L and further to the early, middle and late T dwarfs. Thus the observed characteristics of the SEDs and spectra are reasonably interpreted as the temperature effect by the UCMs. The resulting $T_{\rm eff}$ values are also compared in Table 4 with those obtained from the bolometric fluxes based on the integrated near infrared fluxes, $T_{\rm eff}(f_{\rm bol})$, and on the K band bolomtric correction, $T_{\rm eff}({\rm BC}_K)$, in the separate paper (Nakajima et al. 2004), which applied the same models to obtain the bolometric corrections but emphasized the different aspects of both the observed and predicted data. The agreement of the $T_{\rm eff}$ values based on the different methods is generally fair except for L5 dwarf 2MASS 1507, and this fact may confirm the mutual consistency of our analyses.

As for the L5 dwarf 2MASS 1507, the present spectral analysis shows $T_{\rm eff} \approx 1850$ K while the result based on the bolometric flux shows $T_{\rm eff}$ value as low as 1400 K. One problem is that the same infrared color does not necessarily correspond to the same effective temperature (e.g. Fig. 5) or to the same spectral type (e.g. Kirkpatrick et al. 2000; Leggett et al. 2002),

and this fact implies that the similar SED may result from the different values of $T_{\rm eff}$ or different spectral types. In other words, our result based on the SED is not necessarily a unique solution but there may be a different solution closer to 1400 K.

To examine such a possibility, we compare the observed spectrum of 2MASS 1507 with the predicted ones from the high temperature models ($T_{\rm eff} = 1700 - 1900$ K) in Fig.13a and with those of the low temperature models ($T_{\rm eff} = 1400 - 1600$ K) in Fig.13b. Inspection of Fig.13a suggests that the overall shape of the SEDs as well as the major molecular bands such as of CO and H_2O can reasonably be accounted for by a model with $T_{\rm eff}$ between 1800 and 1900 K and, for this reason, we suggested $T_{\rm eff} \approx 1850$ K in Sect. 4.1 (Fig. 7b). On the other hand, the overall SED appears to be accounted for by a model of $T_{\rm eff} \approx 1400$ K in Fig.13b. However, it also appears that the methane bands at 2.2 μm is predicted to be quite appreciable by this model. This computation of methane bands is based on the linelist of CH_4 (case II) and not due to the overestimation by the band model opacity referred to as case I (see Fig. 9a for the predicted spectrum based on the case I opacity for the 1400 K model). For this reason, we cannot accept the low temperature model for the L5 dwarf 2MASS 1507, and the origin of the discrepant $T_{\rm eff}$ values by the different methods remains unsolved. In conclusion, even though the same infrared color corresponds two different effective temperatures, this degeneracy can be removed in the spectra by considering both the overall shape of the spectrum (or SED) and some molecular features sensitive to temperature (e.g. CH_4).

Also our UCMs were used to interpret the CM diagram such as $(J-K, M_J)$ diagram(Tsuji & Nakajima 2003). For this attempt, there is a severe criticism that the detailed behavior of the models on the CM diagram does not match observations (e.g. Tinney, Burgasser, & Kirkpatrick 2003). However, the point of our present analysis based on UCMs is not the detailed quantitative fits to individual objects, but rather directed to understand the overall behaviors of the colors, magnitudes, SEDs, and spectra throughout L to T dwarfs based on a single sequence of model photospheres. For this purpose, our results provided a possibility of unified understanding of all these observables while the previous models (our models B and C as well as more or less similar models by other authors) could not. As for $(J-K, M_J)$ diagram, the J band flux suffers the most serious effect of dust and the difficulties such as noted in Sects.5.1 and 5.2 must be overcome before we can achieve a better quantitative fit.

Finally, appropriate knowledge on the $p-T$ structure of the photospheres should be vital to analyze high resolution spectra of L and T dwarfs. So far, we have restricted ourselves to examine the effect of $T_{\rm eff}$ and $\log g$ on the spectra, but abundance should certainly be another factor to be considered. For example, observed H_2O bands in SDSS 1750 appeared to be too weak to be explained by the predicted ones (Sect. 4.4), unlike the other objects, and such

a possibility that the oxygen abundance and/or metallicity in SDSS 1750 may be non-solar can be confirmed only by the detailed abundance analyses. Since the line broadenings by turbulence, damping, and other effects must be considered simultaneously for this purpose, quantitative analysis of high resolution spectra should be called for. It is to be noted that the recent progress in the IR spectroscopy finally made it possible to analyze high resolution infrared spectra of faint brown dwarfs (e.g. Smith et al. 2003).

6. CONCLUDING REMARKS

We have shown that the spectra or SEDs of L and T dwarfs can be interpreted consistently by a single grid of UCMs. At present, we cannot yet achieve a fully self-consistent model photosphere of ultracool dwarfs because of the complexities due to the coupling of physico-chemical processes relating to the cloud formation and associated dynamical processes. Instead, we restricted ourselves to a semi-empirical approach which is based only on a simple thermodynamical constraint, and reduced all the possible complicated dynamical effects to a quasi-static model photosphere to be treated by the classical non-grey theory. It is to be noted that the model photosphere itself is not necessarily our final purpose, but our purpose is to understand the real astronomical objects, in this case, L and T dwarfs. The model photosphere is simply a means by which to help this aim, even though better models are certainly more useful for this purpose. Thus the aim of our UCMs is not to provide the exact quantitative fits to observed data at present. It is hoped that our semi-empirical approach can be of some help as a guide to interpret and analyze the observed data of ultracool dwarfs, and hopefully will provide a guideline by which a more physical model can be developed in the near future. To be of some use for this purpose, the numerical data of the UCMs, including the spectra and SEDs, are made available through our Web site [4].

One of the authors (T.T.) would like to thank Sumner Davis for allowing to access his spectroscopic database of molecules including FeH and Hugh Jones for his help on the spectroscopic database of H_2O lines by Partridge & Schwenke. We thank the Subaru staff and all those who have contributed to develop the fine spectrographs as well as the Subaru telescope, with which our observations could have been made possible. We also thank an anonymous referee for helpful comments and suggestions. This work was supported by the grants-in-aid of JSPS Nos.11640227 (T.T.) and 14520232 (T.N.).

[4]http://www.mtk.ioa.s.u-tokyo.ac.jp/~ttsuji/export/ucm

REFERENCES

Ackerman, A. S., & Marley, M. S. 2001, ApJ, 556, 872

Allard, F., Hauschildt, P. H., Baraffe, I., & Chabrier, G. 1996, ApJ, 465, L123

Allard, F., Hauschildt, P. H., Alexander, D. R., Tamani, A., & Schweitzer, A. 2001, ApJ, 556, 357

Allende Prieto, C., Lambert, D. L. & Asplund, M. 2001, ApJ, 556, L63

Allende Prieto, C., Lambert, D. L. & Asplund, M. 2002, ApJ, 573, L137

Anders, E., & Grevesse, N. 1989, Geochim. Cosmochim. Acta, 53, 197

Burgasser, A. J., et al. 2002a, ApJ, 564, 421

Burgasser, A. J., et al. 2002b, ApJ, 571, L151

Burrows, A., et al. 1997, ApJ, 491, 856

Burrows, A., Burgasser, A. J., Kirkpatrick, J. D., Liebert, J., Milson, J. A., Sudarsky, D., & Hubeny, I. 2002, ApJ, 573, 394

Burrows, A., Marley, M. S., & Sharp, C. M. 2000, ApJ, 531, 438

Burrows, A., & Sharp, C. M. 1999, ApJ, 512, 843

Burrows, A., & Volobuyev, M. 2003, ApJ, 583, 985

Cayrel, R., & Jugaku, J. 1963, Ann d' Astrophys, 26, 495

Cooper, C. S., Sudarsky, D., Milson, J. A., Lunine, J. I., & Burrows, A. 2003, ApJ, 586, 1320

Cushing, M. C., Rayner, J. T., Davis, S. P., & Vacca, W. D. 2003, ApJ, 582, 1066

Dahn, C. C., et al. 2002, AJ, 124, 1170

Eriksson, T. S., Hjortsberg, A., Niklasson, G. A., & Granqvist, C. G. 1981, Appl. Opt., 20, 2742

Fegley, B., Jr., & Lodders, K. 1996, ApJ, 472, L37

Geballe, T. R., et al. 2002, ApJ, 564, 466

Geballe, T. R., Kulkarni, S. R., Woodward, C. E., & Sloan, G. C. 1996, ApJ, 467, L101

Hasegawa, H., & Kozasa, T. 1988, Prog. Theor. Phys. Suppl., 96, 107

Helling, Ch., Oevermann, M., Luttke, M. J. H., Klein, R., & Sedlmayr, E. 2001, A&A, 376, 194

Jacquinet-Husson, N., et al. 1999, J. Quant. Spectros. Radiat. Transfer, 62, 205

Johnson, P. B., & Christy, R. W. 1974, Phys. Rev. B, 9, 5056

Jones, H. R. A., & Tsuji, T. 1997, ApJ, 522, L65

Kirkpatrick, J. D., et. al. 1999, ApJ, 519, 802

Kirkpatrick, J. D., et. al. 2000, AJ, 120, 447

Kurucz, R. L. 1993, Kurucz CD-ROM 13, ATLAS 9 Stellar Atmosphere Programs and 2 km s^{-1} Grid (Cambridge: SAO)

Langhoff, S. R., & Bauschlicher, C. W. 1990, J. Mol. Spectrosc., 141, 243

Leggett, S. K., et al. 2000, ApJ, 536, L35

Leggett, S. K., et al. 2002, ApJ, 564, 452

Lenham, A. P., & Treherne, D. M. 1966, in Optical Propeties and Electronic Structure of Metal and Alloys, ed. F. Abelès (Amsterdam: North Holland), 196

Liebert, J., Reid, I. N., Burrows, A., Burgasser, A. J., Kirlpatrick, J. D., & Gizis, J. E. 2000, ApJ, 533, L155

Lodders, K. 1999, ApJ, 519, 793

Lodders, K. 2002, ApJ, 577, 974

Lodders, K., & Fegley, B., Jr. 2002, Icarus, 155, 393

Ludwig, H. -G., Allard, F., & Hauschildt, P. H. 2002, A&A, 395, 99

Marley, M. S. 2000, in ASP Conf. Ser. 212, From Giant Planets to Cool Stars, ed. C. F. Griffith & M. S. Marley (San Francisco: ASP), 152

Marley, M. S., Saumon, D., Guillot, T., Freedman, R., Hubbard, W. B., Burrows, A., & Lunine, J. I. 1996, Science, 272, 1919

Marley, M. S., Seager, S., Saumon, D., Lodders, K., Ackerman, A. S., Freedman, R., & Fan, X. 2002, ApJ, 568, 335

Nakajima, T., Tsuji, T., & Yanagisawa, K. 2001, ApJ, 561, L119

Nakajima, T., Tsuji, T., & Yanagisawa, K. 2004, ApJ(in press)

Noll, K. S., Geballe, T. R., Leggett, S. K., & Marley, M. S. 2000, ApJ, 541, L75

Ordal, M.A., Bell, R.J., Alexander, R. W., Jr. Newrence, L.A., & Query, M. R. 1988, Appl. Opt.. 27, 1203

Ossenkopf, V., Hennings, Th., & Mathis, J. S. 1992, A&A, 261, 567

Partridge, H., & Schwenke, D. W. 1997, J. Chem. Phys., 106, 4618

Phillips, J. G., Davis, S. P., Lindgren, B., & Balfour, W. 1987, ApJS, 65,721

Rothman, L. S. 1997, High-Temperature Molecular Spectroscopic Database (CD-ROM) (Andover: ONTAR Co.)

Schiavon, R.P., Barbuy,B., & Singh,P.D. 1997, ApJ, 484, 499

Schweitzer, A., Gizis, J. E., Hauschildt, P. H., Allard, F., & Reid, I. N. 2001, ApJ, 555, 368

Simon, D. A., & Tokunaga, A. T. 2002, PASP, 114, 169

Smith, V. V., et al. 2003, ApJ, 599, L107

Tinney, C. G., Burgasser, A. J., & Kirkpatrick, J. D. 2003, AJ, 126, 975

Tokunaga, A. T., Simon, D. A., & Vacca, W. D. 2002, PASP, 114, 180

Tsuji, T. 2000, in Very Low-Mass Stars and Brown Dwarfs, ed. R. Rebolo & M. R. Zapatero-Osorio (New York: Cambridge Univ. Press), 156

Tsuji, T. 2001, in Ultracool Dwarfs - New Spectral Types L and T, ed. H. R. A. Jones & I. A. Steele (Berlin: Springer-Verlag), 9

Tsuji, T. 2002, ApJ, 575, 264 (Paper I)

Tsuji, T. 2003, in IAU Symp. 211 Brown Dwarfs ed. E. Martín, (San Francisco: ASP), 361

Tsuji, T., & Nakajima, T. 2003, ApJ, 585, L151

Tsuji, T., Ohnaka, K., & Aoki, W. 1996a, A&A, 305, L1

Tsuji, T., Ohnaka, K., & Aoki, W. 1999, ApJ, 520, L119

Tsuji, T., Ohnaka, K., Aoki, W., & Nakajima, T. 1996b, A&A, 308, L29

Unsöld, A. 1955, Physik der Sternatmosphären, zweiten Auflage, (Berlin: Springer-Verlag)

van de Hulst, H. C. 1957, Light Scattering by Small Particles (New York: Wiley)

Wallace, L., & Hinkle, K. 2001, ApJ, 559, 424

Weast, R. C. 1985-86, CRC Handbook of Chemistry and Physics (Boca Raton: CRC Press)

Woitke, P., & Helling, Ch. 2003, A&A, 399, 297

Table 1: PHYSICL PARAMETERS OF DUST GRAINS

dust species	a_0 (Å)[a]	σ (dyn cm^{-1})[a]	$\rho_{\rm dust}$ (gr cm^{-3})[b]	n^{*}[c]	$r_{\rm cr}$ (Å)[c]	$Q_{\rm ext}$ & γ[d]
corundum (Al_2O_3)	1.7179	690	4.022	3.2×10^5	118	1
iron (Fe)	1.4114	1800	7.874	1.7×10^6	171	2, 3, 4
enstatite ($MgSiO_3$)	2.3193	400	3.209	3.8×10^5	168	5

[a] Hasegawa & Kozasa (1988)

[b] Weast (1985-86)

[c] for the supersaturation ratio $S = 1.1$

[d] Numerical results (Table 2) are based on the optical constants by: (1) Eriksson et al. 1981; (2) Lenham & Treherne 1966; (3) Johnson & Christy 1974; (4) Ordal et al. 1988; (5) Ossenkopf, Hennings, & Mathis 1992.

Table 2: EFFICIENCY FACTOR FOR EXTINCTION AND ALBEDO ($r = 0.01\mu$m)

λ	iron		enstatite		corundum	
(μm)	$\log Q_{\rm ext}$	γ	$\log Q_{\rm ext}$	γ	$\log Q_{\rm ext}$	γ
0.100	0.520	0.251	-0.385	0.130	-1.140	1.000
0.300	-0.341	0.090	-1.192	0.051	-2.738	0.795
0.500	-1.095	0.008	-1.821	0.009	-3.649	0.354
0.700	-1.334	0.004	-2.080	0.004	-3.733	0.120
0.900	-1.545	0.002	-2.224	0.002	-3.788	0.061
1.100	-1.707	0.002	-2.290	0.002	-3.805	0.022
1.300	-1.836	0.002	-2.307	0.001	-3.807	0.012
1.500	-1.964	0.002	-2.339	0.000	-3.825	0.006
1.700	-2.092	0.001	-2.400	0.000	-3.785	0.004
2.000	-2.285	0.001	-2.469	0.000	-3.725	0.002
3.000	-2.765	0.000	-2.742	0.000	-3.525	0.000
4.000	-3.076	0.000	-2.913	0.000	-3.439	0.000
5.000	-3.320	0.000	-3.009	0.000	-3.460	0.000
6.000	-3.528	0.000	-3.045	0.000	-3.267	0.000
7.000	-3.684	0.000	-3.031	0.000	-3.173	0.000
8.000	-3.834	0.000	-2.901	0.000	-3.095	0.000
9.000	-3.924	0.000	-2.421	0.000	-3.002	0.000
10.000	-4.005	0.000	-2.067	0.000	-2.464	0.000
11.000	-4.202	0.000	-2.219	0.000	-1.936	0.000
12.000	-4.399	0.000	-2.464	0.000	-1.716	0.000
13.000	-4.535	0.000	-2.656	0.000	-1.837	0.000
14.000	-4.612	0.000	-2.684	0.000	-1.987	0.000
15.000	-4.677	0.000	-2.683	0.000	-2.117	0.000
20.000	-4.934	0.000	-2.575	0.000	-2.553	0.000
25.000	-5.097	0.000	-2.801	0.000	-2.690	0.000
30.000	-5.210	0.000	-2.923	0.000	-2.945	0.000
35.000	-5.297	0.000	-3.060	0.000	-3.123	0.000
40.000	-5.369	0.000	-3.171	0.000	-3.236	0.000
45.000	-5.429	0.000	-3.275	0.000	-3.349	0.000
50.000	-5.483	0.000	-3.380	0.000	-3.462	0.000

Table 3: LOGARITHMS OF THE INTEGRATED FLUXES OVER THE FILTER BANDS (MKO SYSTEM)

$\log g$	$T_{\rm eff}$ (K)	$\log F_J$	$\log F_H$	$\log F_K$	$T_{\rm eff}$ (K)	$\log F_J$	$\log F_H$	$\log F_K$
4.5	700.	5.902	5.513	5.034	800.	6.159	5.741	5.349
	900.	6.364	5.959	5.622	1000.	6.542	6.171	5.853
	1100.	6.675	6.406	6.072	1200.	6.757	6.667	6.301
	1300.	6.832	6.881	6.522	1400.	6.860	7.036	6.776
	1500.	6.908	7.138	6.981	1600.	6.919	7.209	7.152
	1700.	7.130	7.354	7.252	1800.	7.338	7.459	7.319
	1900.	7.486	7.532	7.344	2000.	7.623	7.616	7.405
	2100.	7.716	7.688	7.466	2200.	7.782	7.764	7.547
	2300.	7.840	7.833	7.617	2400.	7.899	7.902	7.685
	2500.	7.954	7.969	7.747	2600.	8.008	8.035	7.807
5.0	700.	5.895	5.632	5.016	800.	6.161	5.858	5.348
	900.	6.378	6.064	5.620	1000.	6.555	6.266	5.859
	1100.	6.683	6.485	6.089	1200.	6.780	6.702	6.303
	1300.	6.846	6.902	6.522	1400.	6.884	7.058	6.760
	1500.	6.885	7.152	7.000	1600.	6.923	7.228	7.165
	1700.	7.022	7.330	7.278	1800.	7.227	7.449	7.351
	1900.	7.419	7.540	7.391	2000.	7.562	7.620	7.437
	2100.	7.695	7.706	7.482	2200.	7.791	7.780	7.537
	2300.	7.865	7.848	7.596	2400.	7.919	7.916	7.669
	2500.	7.969	7.979	7.735	2600.	8.018	8.041	7.797
5.5	700.	5.867	5.713	4.943	800.	6.146	5.951	5.328
	900.	6.374	6.152	5.608	1000.	6.558	6.343	5.849
	1100.	6.699	6.540	6.074	1200.	6.795	6.743	6.300
	1300.	6.861	6.930	6.523	1400.	6.910	7.076	6.743
	1500.	6.940	7.183	6.962	1600.	6.974	7.260	7.139
	1700.	7.038	7.346	7.274	1800.	7.155	7.428	7.358
	1900.	7.366	7.529	7.403	2000.	7.536	7.617	7.437
	2100.	7.666	7.699	7.479	2200.	7.772	7.781	7.530
	2300.	7.856	7.855	7.587	2400.	7.925	7.922	7.648
	2500.	7.983	7.987	7.712	2600.	8.030	8.048	7.779
3.95	9550.	9.330	9.182	8.799				

Table 4: EFFECTIVE TEMPERATURES

Object	Sp. type	$T_{\rm eff}$(SED)	$T_{\rm eff}(f_{\rm Bol})$	$T_{\rm eff}({\rm BC}_K)$
2MASS 1146+22A	L3	1900 K	1612-1748 K	2098-2276 K
2MASS 1507-16	L5	1850	1371-1487	1544-1675
SDSS 2249+00	L5	1800		
2MASS 1711+22	L6.5	1800		
2MASS 0920+35	L6.5	1800		
2MASS 1523+30	L8	1500	1287-1395	1330-1442
SDSS 1254-01	T2	1300	1252-1358	1279-1387
			1348-1462	1348-1462
SDSS 1750+17	T3.5	1100		
Gl229B	T6	900	905-981	928-1007
2MASS 1217-03	T7.5	800	885-960	873-947

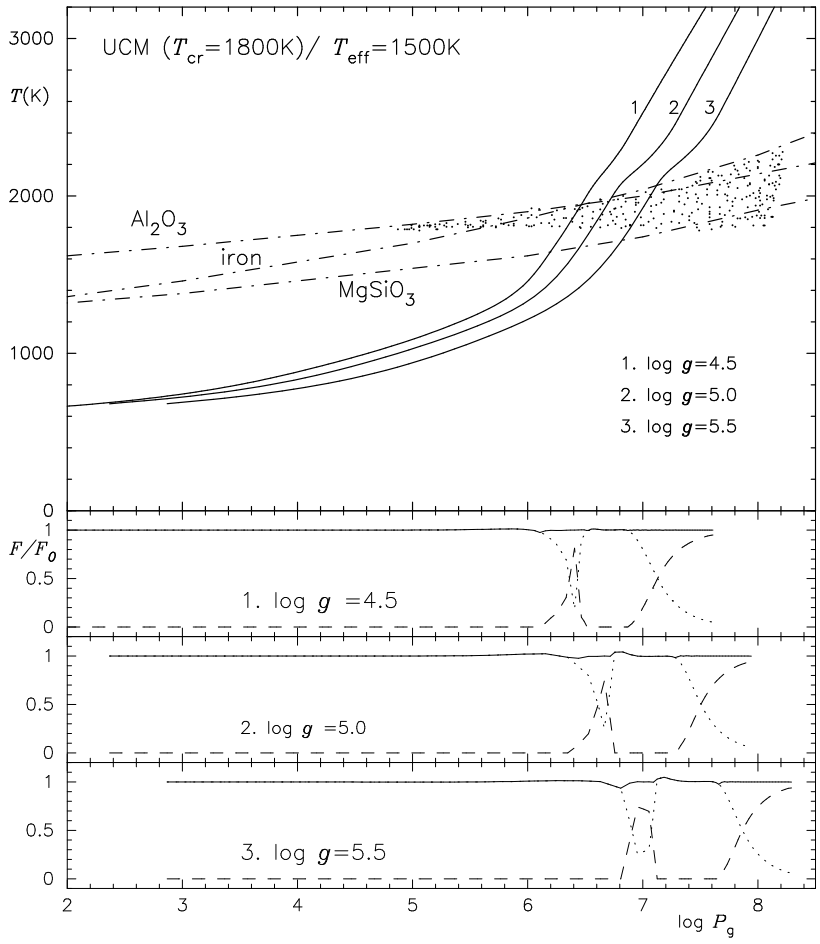

Fig. 1.— The unified cloudy models of $T_{\rm eff}$ = 1500K are shown in the upper panel for three values of the surface gravities; log g = 4.5, 5.0 and 5.5 ($v_{\rm micro}$ =1 km s^{-1} and the solar metallicity). The dot-dashed curves are the dust condensation lines for corundum, iron, and enstatite. The lower three panels show the radiative, convective, and total fluxes normalized by $\sigma T_{\rm eff}^4/\pi$ by the dotted, dashed, and solid lines, respectively, for three values of log g.

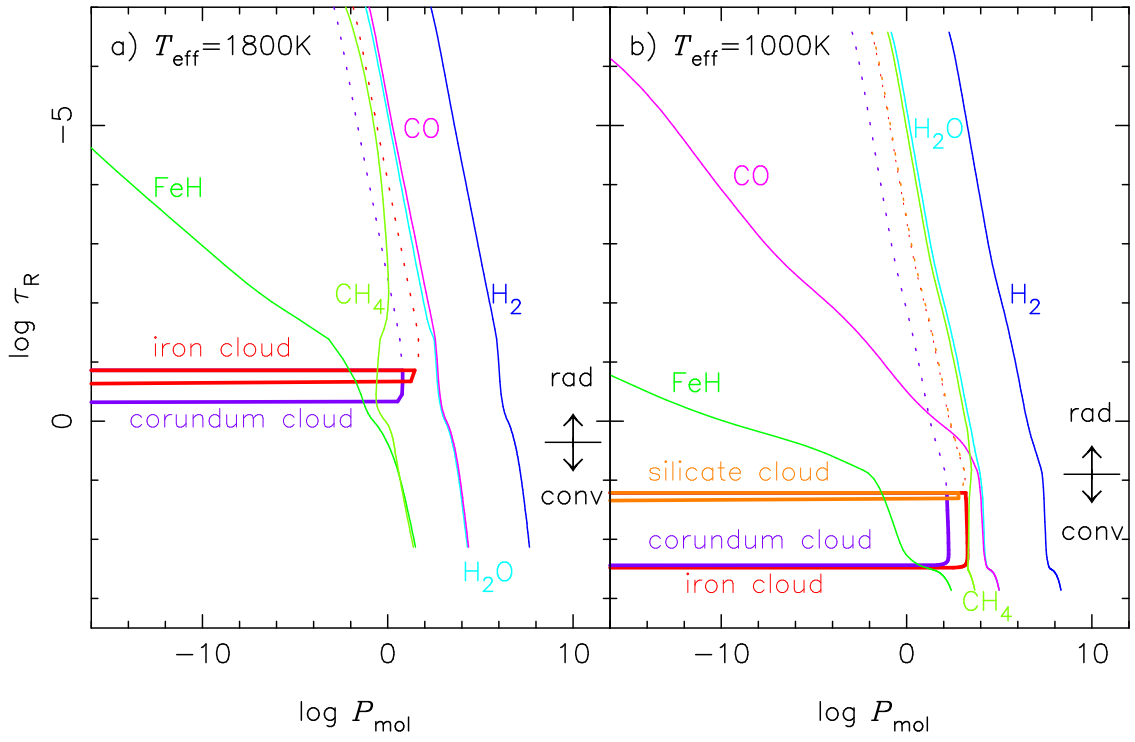

Fig. 2.— a) Logarithms of the partial pressures (dyn cm^{-2}) of some molecules (abscissa) are plotted against $\log \tau_{\rm R}$ (ordinate) in the UCM ($T_{\rm cr} = 1800$ K) of $T_{\rm eff} = 1800$ K and $\log g$ =5.0. A thin iron cloud and a geometrically thicker cloud of corundum are formed in the optically thin region. The abundances of the dust grains are shown by the fictitious pressures of nuclei of the refractive elements locked in the dust grains (i.e. Fe and Al for iron and corundum, respectively). The dust abundances under the strict thermodynamical equilibrium are shown by the dashed lines. The radiative and convective regimes are indicated. b) The same for the UCM of $T_{\rm eff} = 1000$ K and $\log g$ =5.0. The iron, corundum, and silicate clouds are formed but in the optically thick region.

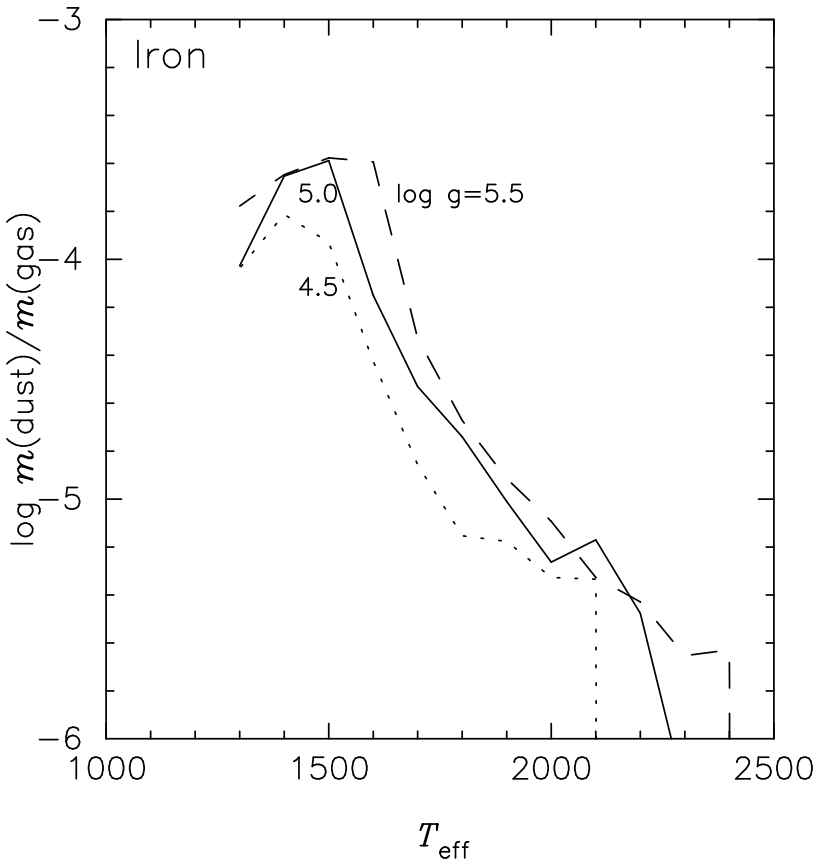

Fig. 3.— The ratio of the dust mass column density m(dust) to the total gas mass density m(gas) in the observable photosphere ($\tau_{\rm R} \lesssim 3$ in UCMs with $T_{\rm cr} = 1800\,{\rm K}$) is shown in logarithmic scale against $T_{\rm eff}$ for $\log g = 4.5$, 5.0, and 5.5 by dotted, solid, and dashed lines, respectively.

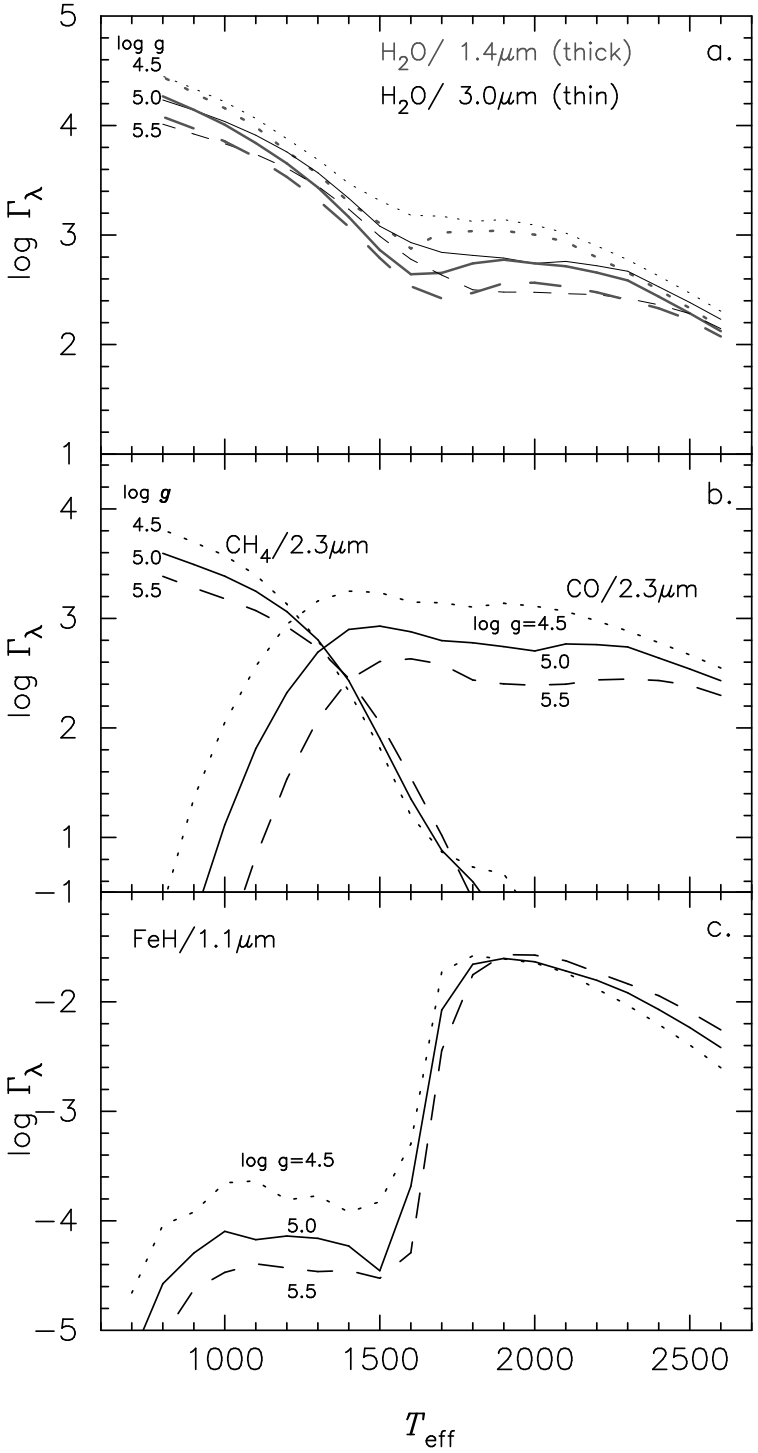

Fig. 4.— a) The predicted line intensities in logarithmic scale for a line of $\chi = 0.0$eV of the H_2O 1.4 (thick lines) and 3.0 μm (thin lines) bands plotted against $T_{\rm eff}$ for UCMs ($T_{\rm cr} = 1800$ K) with $\log g = 4.5$, 5.0, and 5.5 by dotted, solid, and dashed lines respectively. b) The same as for a), but for the CH_4 2.3 μm and CO 2.3 μm bands. c) The same as for a), but for the FeH 1.1 μm bands.

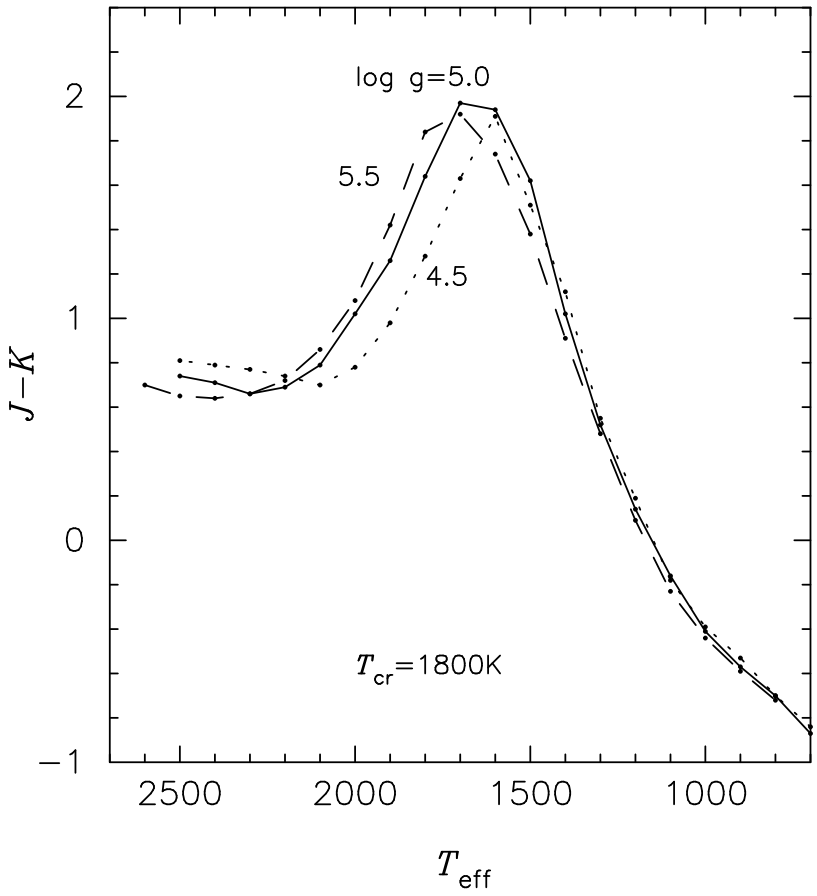

Fig. 5.— The predicted $J - K$ color (MKO system) is plotted against $T_{\rm eff}$ for UCMs ($T_{\rm cr} = 1800\,{\rm K}$) with $\log g = 4.5$, 5.0, and 5.5 by dotted, solid, and dashed lines, respectively.

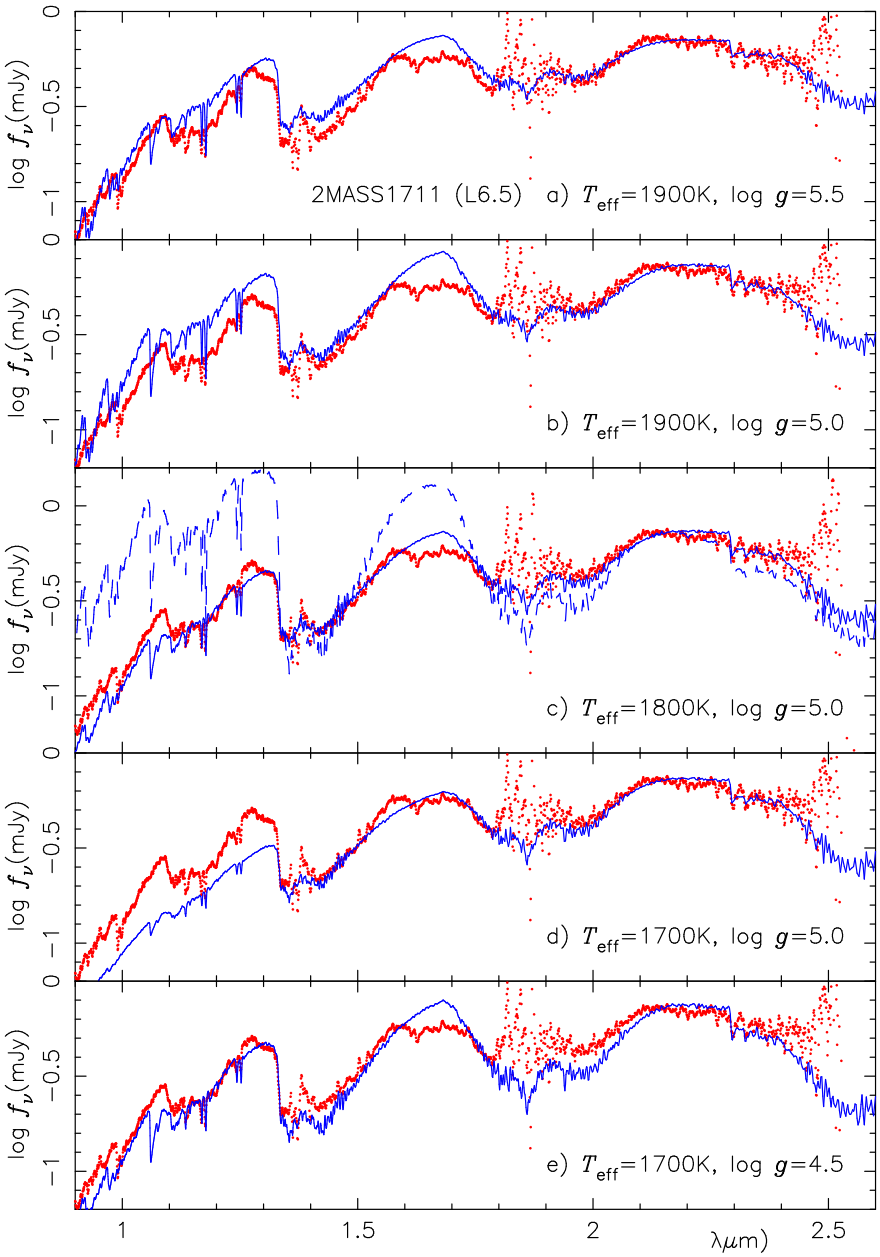

Fig. 6.— Observed spectrum of the L6.5 dwarf 2MASS 1711+22 (filled circles) is compared with the predicted ones (solid lines) based on the UCMs ($T_{\rm cr}$ = 1800 K): a) $T_{\rm eff}$ = 1900 K and $\log g$ =5.5. b) $T_{\rm eff}$ = 1900 K and $\log g$ =5.0. c) $T_{\rm eff}$ = 1800 K and $\log g$ =5.0. The dashed line shows the predicted spectrum based on the model of the same parameters but all the dust grains are segregated and precipitated below the photosphere (case C). The difference between the solid and dashed lines indicates the effect of the dust clouds. d) $T_{\rm eff}$ = 1700 K and $\log g$ =5.0. e) $T_{\rm eff}$ = 1700 K and $\log g$ =4.5.

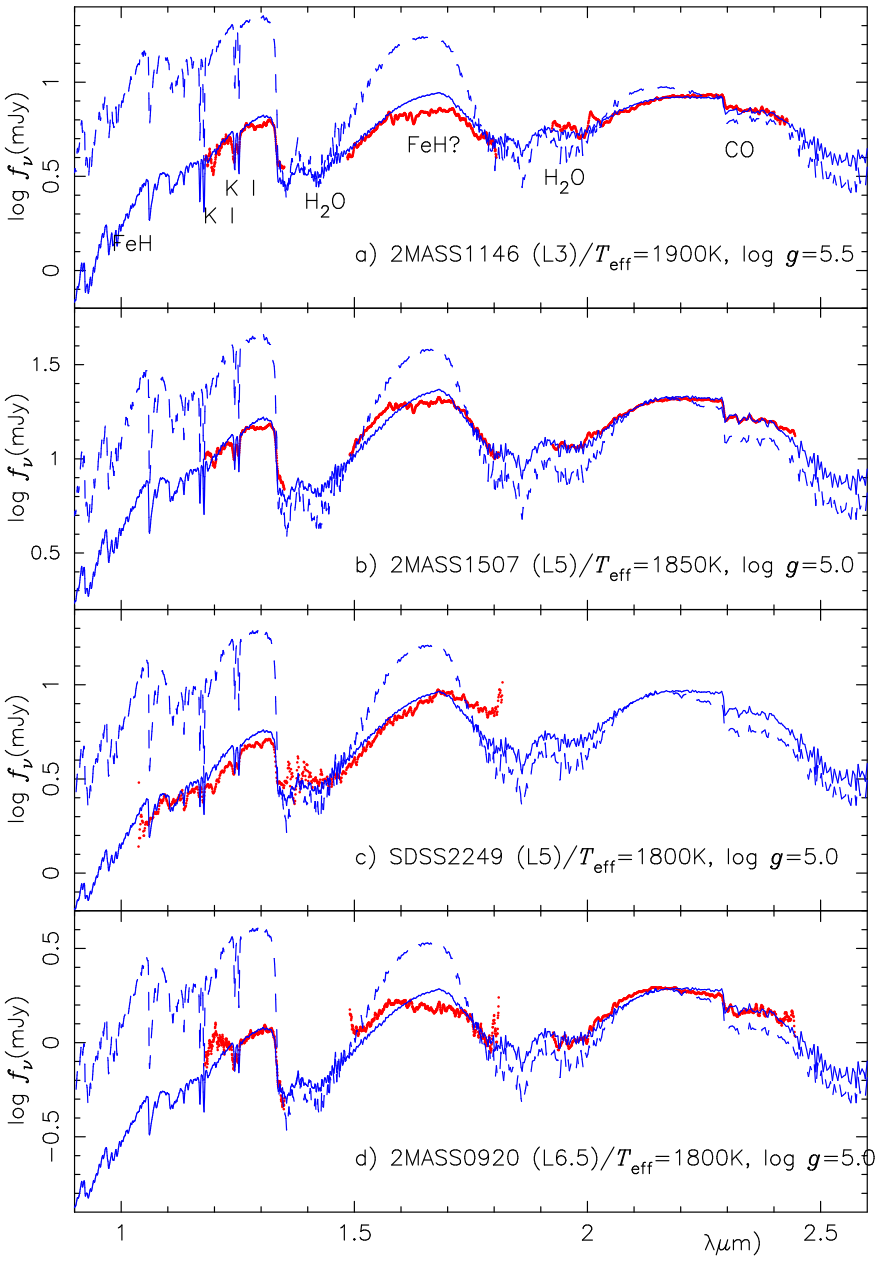

Fig. 7.— Observed spectra (filled circles) of middle L dwarfs are compared with the predicted ones (solid lines) based on UCMs ($T_{\rm cr}$ = 1800 K). The dashed lines have the same meaning as that in Fig. 6c: a) 2MASS 1146+22 (L3) vs. UCM with $T_{\rm eff}$ = 1900 K and $\log g$ =5.5. b) 2MASS 1507-16 (L5) vs. UCM with $T_{\rm eff}$ = 1850 K and $\log g$ =5.0. c) SDSS 2249+00 (L5) vs. UCM with $T_{\rm eff}$ = 1800 K and $\log g$ =5.0. d) 2MASS 0920+35 (L6.5) vs. UCM with $T_{\rm eff}$ = 1800 K and $\log g$ =5.0.

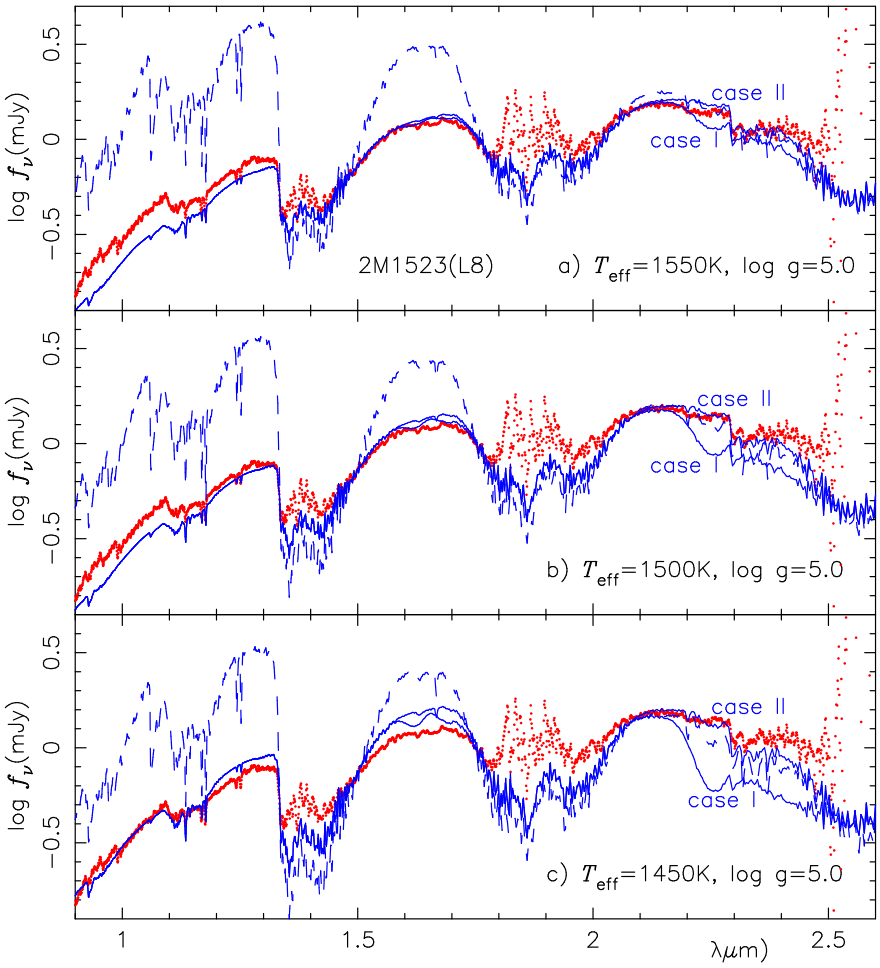

Fig. 8.— Observed spectrum (filled circles) of the late L dwarf 2MASS 1523+30 (L8) is compared with the predicted ones (solid lines) based on UCMs ($T_{\rm cr}$ = 1800 K) of: a) $T_{\rm eff}$ = 1550 K and $\log g$ =5.0, b) $T_{\rm eff}$ = 1500 K and $\log g$ =5.0, and c) $T_{\rm eff}$ = 1450 K and $\log g$ =5.0. Note that the predicted spectra show bifurcations in the region of methane bands near 1.6 and 2.2 μm according as the cases I (band model opacity) or II (linelist) opacities are used for CH_4. The dashed lines have the same meaning as that in Fig. 6c and only the results based on the case II opacity are shown.

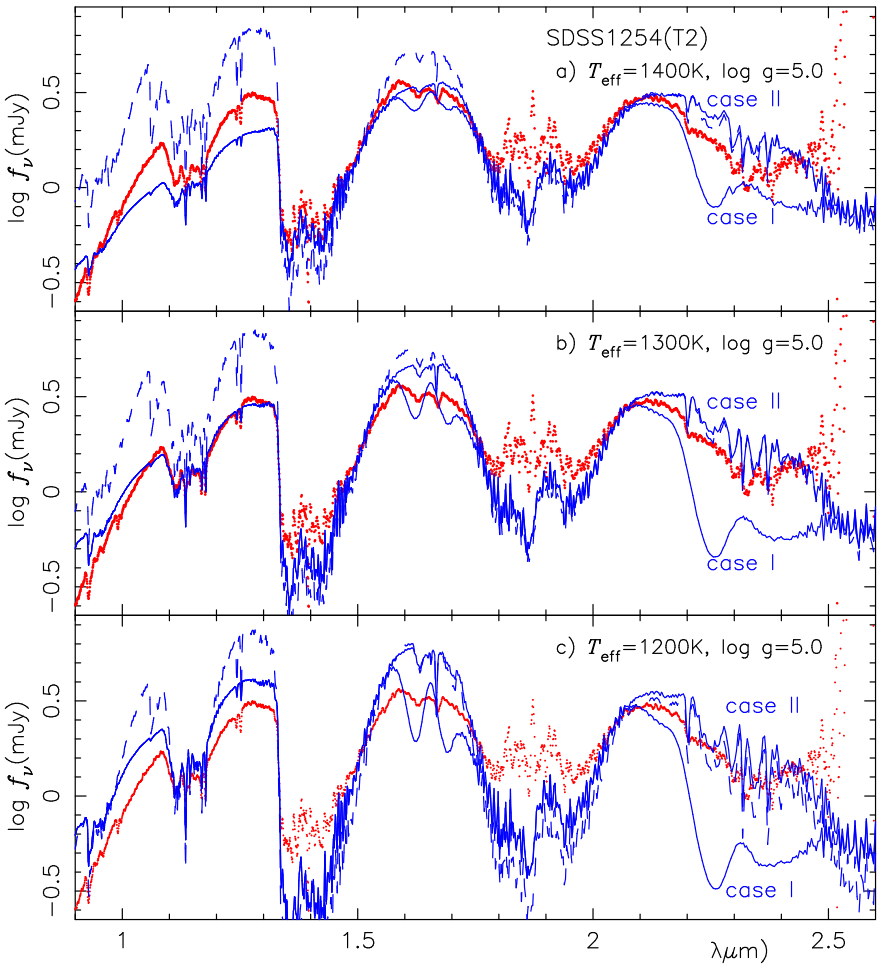

Fig. 9.— Observed spectrum (filled circles) of the early T dwarf SDSS 1254-01 (T2) is compared with the predicted ones (solid lines) based on UCMs ($T_{\rm cr} = 1800\,{\rm K}$) of: a) $T_{\rm eff} = 1400\,{\rm K}$ and $\log g$ =5.0, b) $T_{\rm eff} = 1300\,{\rm K}$ and $\log g$ =5.0, and c) $T_{\rm eff} = 1200\,{\rm K}$ and $\log g$ =5.0. See the legend of Fig.8 as for dashed lines and for bifurcations of the solid lines.

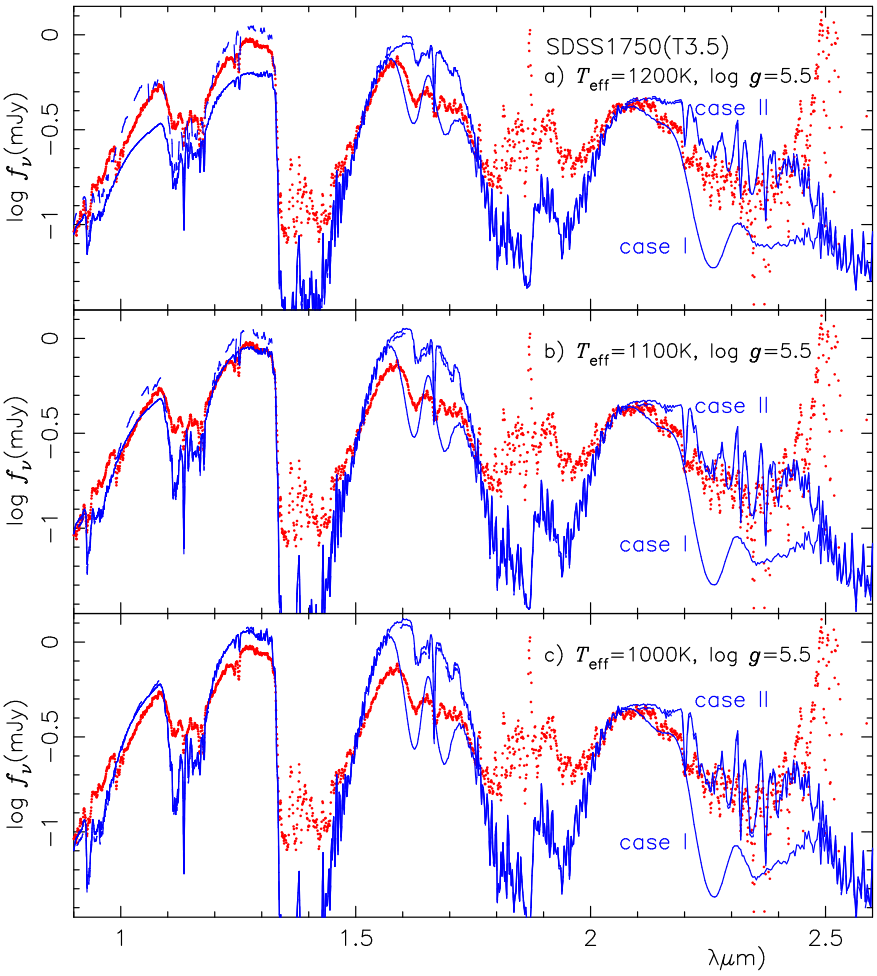

Fig. 10.— Observed spectrum (filled circles) of the middle T dwarf SDSS 1750+17 (T3.5) is compared with the predicted ones (solid lines) based on UCMs ($T_{\rm cr}$ = 1800 K) of: a) $T_{\rm eff}$ = 1200 K and $\log g$ =5.5, b) $T_{\rm eff}$ = 1100 K and $\log g$ =5.5, and c) $T_{\rm eff}$ = 1000 K and $\log g$ =5.5. The solid lines are now closer to the dashed lines showing the predicted spectra from the cloud cleared models, and this fact implies that the effect of the dust clouds is diminishing according as the clouds are immersing deeper in the photospheres.

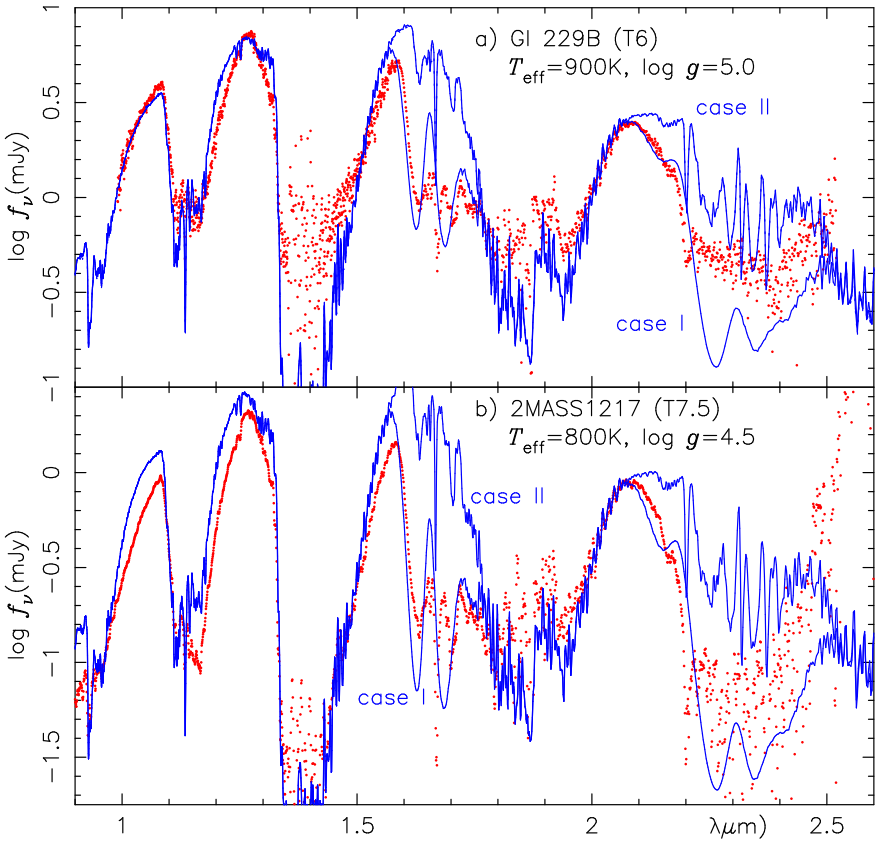

Fig. 11.— Observed spectra (filled circles) of late T dwarfs are compared with the predicted ones (solid lines) based on UCMs ($T_{\rm cr} = 1800\,{\rm K}$): a) Gl229B (T6) vs. predicted spectrum by the model of $T_{\rm eff} = 900\,{\rm K}$ and $\log g$ =5.0. b) 2MASS 1217-03 (T7.5) vs. predicted spectrum by the model of $T_{\rm eff} = 800\,{\rm K}$ and $\log g = 4.5$. Note that the dashed and solid lines are almost overlapping and this means that there is almost no effect of the dust clouds on the emergent spectra predicted from the UCMs.

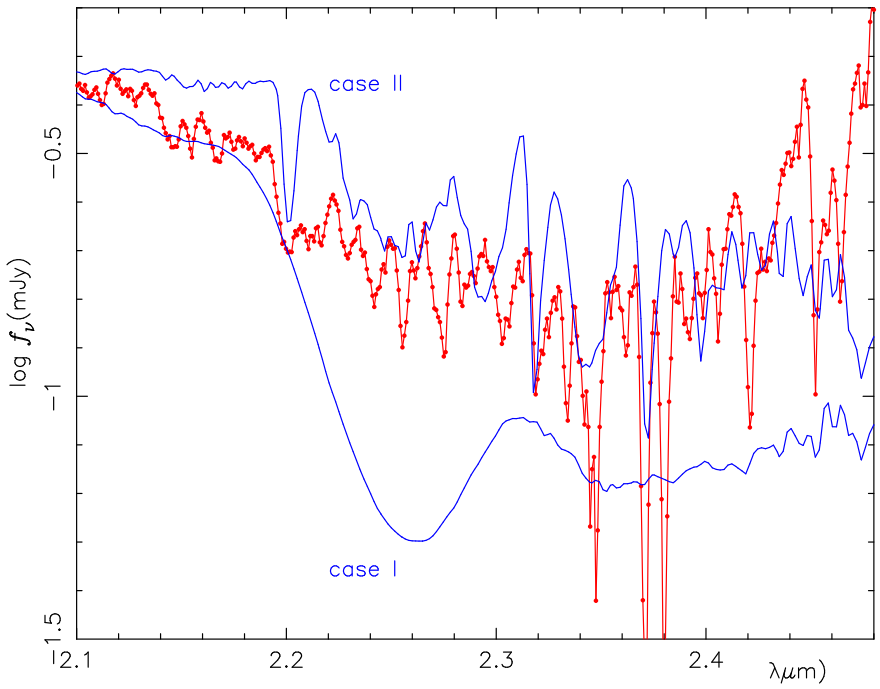

Fig. 12.— Some details of the observed methane spectrum of the T3.5 dwarf SDSS 1750+17 (filled circles connected by the solid line) compared with the predicted ones (solid lines) based on UCMs ($T_{\rm cr}$ = 1800 K) of $T_{\rm eff}$ = 1100 K and $\log g$ =5.5 by the use of the cases I (band model) and II (linelist) methane opacities.

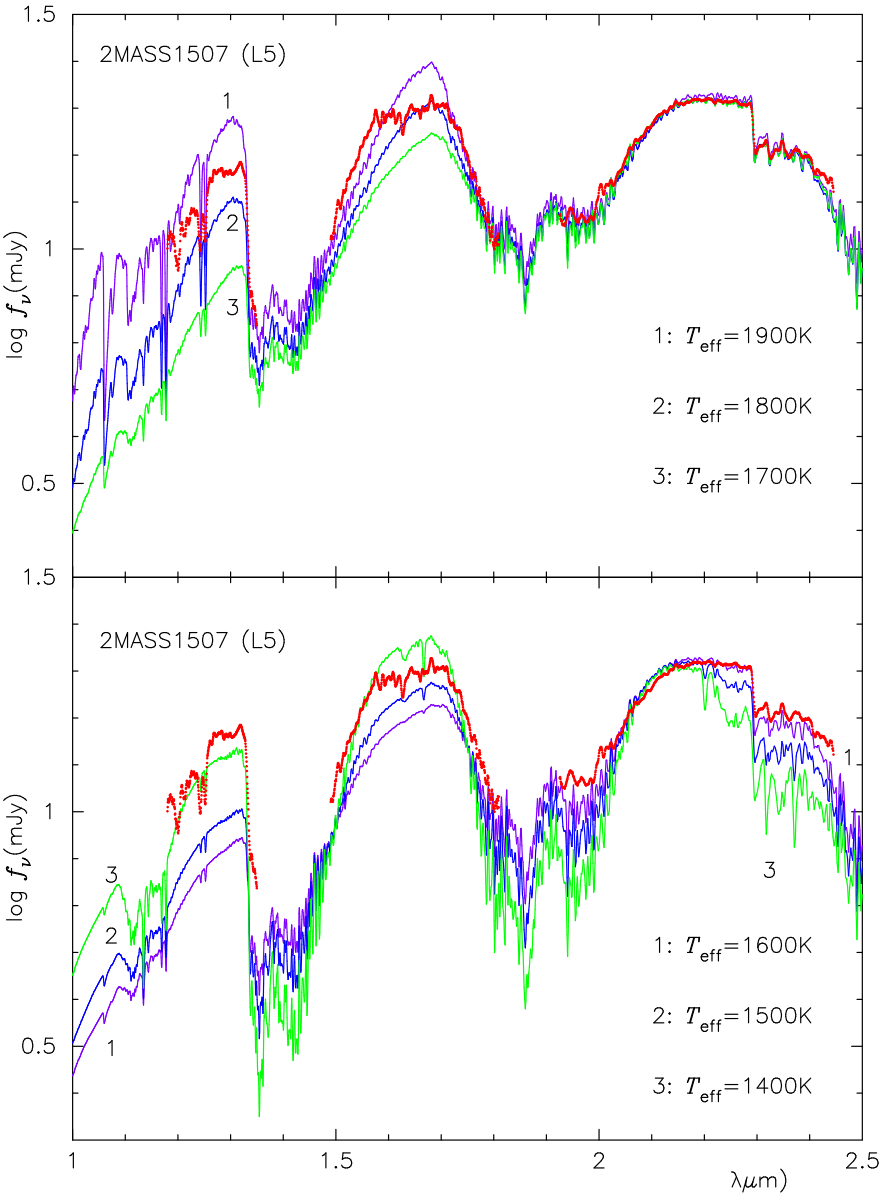

Fig. 13.— Possible two solutions for the spectrum of the L5 dwarf 2MASS 1507-16 (filled circles) are examined by the comparisons with the predicted spectra (solid lines) of: a) Some relatively warm models with $T_{\rm eff} = 1700 - 1900\,{\rm K}$ ($\log g = 5.0$). The warmer models show less depression of the J flux by the dust extinction because the dust column density is still not so large and we suggested $T_{\rm eff} \approx 1850\,{\rm K}$ (Fig.7b). b) Some relatively cool models with $T_{\rm eff} = 1400 - 1600\,{\rm K}$ ($\log g = 5.0$). The cooler models show less depression of the J flux by the dust extinction because of the increased molecular gas above the clouds which are gradually immersing to the invisible region in these $T_{\rm eff}$ range. Although the overall SED can be fitted with the model of $T_{\rm eff} \approx 1400\,{\rm K}$, this models shows too strong methane bands to be matched with observation, and this solution cannot be accepted.